Dynamics of Electronic Rydberg Wave Packets in the Presence of Laser-induced Core Transitions

O. Zobay and G. Alber

Theoretische Quantendynamik, Fakultät für Physik, Universität Freiburg,
D-79104 Freiburg im Breisgau, Germany

Abstract

Recent theoretical work on the dynamics of electronic Rydberg wave packets under the influence of laser-induced core transitions is reviewed. The discussion focuses on the intricate interplay between laser-modified electron correlation effects, radiative damping by the ionic core and the time evolution of electronic Rydberg wave packets. Via the stimulated light force this interplay manifests itself also in the atomic center of mass motion. A unified theoretical framework is provided by combining methods of quantum defect theory, stochastic techniques and semiclassical path expansions.

1.   Introduction

The investigation of physical systems which are situated on the border between the microscopic and the macroscopic regime is of crucial importance for our understanding of quantum mechanics and has therefore received considerable attention both in atomic physics and in quantum optics within the past decades. Due to their large spatial extension in comparison with the Bohr radius $a_0 = 5.3 \cdot 10^{-11}$ m, which sets the characteristic length scale for atomic and molecular quantum phenomena, electronic Rydberg systems are well suited for this purpose. The interplay between classical and quantum mechanical aspects in their behavior is revealed in a particular clear and appealing way in explicitly time-dependent settings. This has been a main impetus for numerous recent studies on the dynamics of electronic Rydberg wave packets [1]. As a major result it has been demonstrated that far away from the atomic nucleus their time evolution is dominated by classical aspects of the electronic motion under the influence of the Coulomb field of the positively charged ionic core and possibly of additional external fields. Quantum aspects manifest themselves mainly in the interference of the probability amplitudes associated with the classical trajectories. Consequently, semiclassical methods have proven successful for an adequate theoretical description of the electronic time evolution in the spatial region outside the atomic core. Inside the core region, however, the dynamics is dominated by processes which are intrinsically of quantum mechanical nature. An example is provided by the electron correlation effects which lead to scattering of a Rydberg electron by the core and to autoionization. These effects are appropriately described within the language of quantum defect theory (QDT) [2, 3, 4].

At present, the behavior of Rydberg wave packets is well examined and well understood in many respects. Experimentally, for example, radially and angularly localized wave packets have been investigated [5, 6], the phenomenon of quantum mechanical revivals has been

demonstrated [7] and the influence of external magnetic and electric fields has been studied [8, 9]. On the theoretical side, semiclassical methods and QDT have been combined in the form of *semiclassical path expansions* [1, 10, 11] to provide a convenient and flexible means for the description of Rydberg wave packet dynamics. Before this background the purpose of the present article consists in demonstrating that the consideration of isolated core excitation (ICE) processes [12] may offer new perspectives in the study of electronic Rydberg wave packets. To this end we review some recent theoretical work in which the wave packet dynamics is examined from various physical points of view. The topics discussed include the coherent modifications of wave packet dynamics by laser-modified electron correlation effects, the dissipative influence of spontaneous emission on wave packets and the connection between electronic wave packet dynamics and atomic center-of-mass motion. The purpose of these investigations is twofold: on the one hand, isolated core excitations in intense laser fields offer the possibility to study manifestations of laser-modified two-electron correlations in electronic wave packet dynamics. Thereby, new effects may arise which are not observed with typical electrostatic configuration interactions [13, 14]. On the other hand, the presented results extend previous work on quantum optical applications of atomic systems with a high density of states [15, 16, 17]. It is expected that the complex electronic dynamics of such systems offers new and interesting possibilities in this context.

Isolated core excitations constitute a specific kind of interaction of a laser field with a Rydberg atom. They play an important role as a spectroscopic tool nowadays [18]. In particular, ICE processes have been used successfully for systematic studies of highly excited autoionizing states of two-electron-like atoms. Basically, an ICE process consists in exciting two atomic valence electrons in an optical two-step process. At first one valence electron is excited to a Rydberg state with one or several laser pulses. Subsequently, a further laser pulse excites the other valence electron to an energetically low lying state of the ionic core. The Rydberg electron acts as a spectator and can be affected by laser-induced core transitions of the second, strongly bound core electron only by the process of shakeup. This shakeup of the Rydberg electron is brought about by a difference of the quantum defects of the two Rydberg series associated with the almost resonantly coupled core states. Early work on ICE processes [18] has concentrated on weak excitations in which the laser-induced transitions of the strongly bound core electron can be described perturbatively. In contrast to these studies, nonperturbative core effects have received some attention only relatively recently [19, 20, 21, 22, 23, 24, 25, 26]. In the following we review some of the recent work on such nonperturbative laser-induced ICE processes and their influence on electronic Rydberg wave packets.

In Sec. 2 elementary principles of ICE processes and of their theoretical description by quantum defect theory (QDT) are summarized [12, 27, 28]. With the help of the concept of photon-dressed core channels [19] these theoretical methods are generalized to cases in which the influence of laser-induced transitions of the strongly bound valence electron cannot be described perturbatively. Combining this theoretical treatment with semi-classical path representations [1] for the dynamics of the excited Rydberg electron a simple and physically transparent description of ICE processes in intense laser fields and their effect on electronic Rydberg wave packets is obtained [29]. Various examples are discussed which demonstrate the influence of the resulting laser-modified electron correlations on the dynamics of electronic Rydberg wave packets. A particularly interesting effect of this kind is the recently studied suppression of autoionization by synchronizing the mean classical orbit time of an electronic Rydberg wave packet with the Rabi period of a resonantly driven ionic core transition [30].

In the context of wave packet dynamics in Rydberg systems the study of dissipative and stochastic influences which destroy quantum coherences has not yet received much attention. Definitely, to some extent this may be attributed to the fact that due to the high level

density of Rydberg systems the solution of the relevant master equations constitutes a diffi-cult mathematical and numerical problem. In ICE processes such a decohering influence on the dynamics of an electronic Rydberg wave packet arises naturally by the radiative decay of the tightly bound core electron. In Sec. 3 recent results [31] on effects of radiative damp-ing in ICE processes are discussed. It is shown that with the help of a decomposition of the relevant master (optical Bloch) equation into N-photon contributions and the application of semiclassical path representations a practical and physically transparent theoretical descrip-tion can be developed. On the basis of this theoretical treatment physical insight is obtained into the intricate interplay between laser-modified electron correlation effects and the spon-taneous emission of photons by the ionic core which is of a stochastic nature and tends to destroy quantum coherences. Examples are presented which analyze the effects the radiative damping of the core transition has on the laser-induced suppression of autoionization. Furthermore, the influence of an electronic Rydberg wave packet on the process of photon emission by the ionic core is discussed.

Motivated by recent investigations in the field of atom optics [32, 33] in Sec. 4 the influ-ence of intense field ICE processes on the atomic center of mass motion is investigated. In general, the large mass difference between an atomic nucleus and its electrons implies that momentum can be transferred from a laser field to the atomic center of mass essentially only by excitation of the internal electronic degrees of freedom. The resulting strong correla-tions between the internal electronic dynamics of an atom and its center of mass motion offer the possibility to deflect atoms in a controlled way by an appropriate choice of the electronic excitation process. For these purposes laser-induced two electron excitation pro-cesses and in particular ICE processes might offer interesting new perspectives. In order to work out main aspects of the intricate, coherent interplay between laser-modified electron correlation effects and their influence on the atomic center of mass motion the discussion focuses on effects arising from the stimulated light force [34, 35].

2.   Isolated Core Excitation in Intense Laser Fields

2.1.   Basic principles of isolated core excitation

A laser field impinging on a Rydberg atom may interact not only with the Rydberg electron but also with the residual ionic core. This latter type of interaction usually proceeds in the form of an isolated core excitation (ICE) which is characterized by the fact that the Ryd-berg electron does not participate directly in the interaction between laser field and core [12, 18]. Isolated core excitations have been studied extensively in the alkaline earth ele-ments Mg, Ca, Sr, and Ba as the corresponding singly-charged ions are excited easily with laser fields in the optical or near-uv regime. An example for a typical ICE process is shown schematically in Fig. 1 for the case of Mg: in a first step, the atom is excited from the $|3s^2\rangle$ ground state to a Rydberg state $|3snd\rangle$ by a two-photon absorption process. The atom thus consists of the $Mg^+(3s)$ ionic core and the nd-Rydberg electron which orbits around the nucleus thereby keeping a large distance from it most of the time. By applying a further laser pulse tuned to a resonance of the Mg^+ ion, e.g. $3s \rightarrow 3p$, the core may now be stimulated to make a transition to an excited state. In comparison to the interaction with the core the direct effects of the laser field on the Rydberg electron, i.e. photoionisation, is negligible. However, the transition process exerts an indirect influence onto the electron which is brought about by correlation effects: as soon as th core is excited the Rydberg electron sense a different short range core potential to which it has to accommodate. This means that generally it cannot remain in a stationary state (i.e., it experiences a "shakeup"). Instead, its wave function transforms into a superposition state which is obtained essentially by the projection of the initial Rydberg state $|nd\rangle$ onto the Rydberg eigenstates $|n'd\rangle$ of the
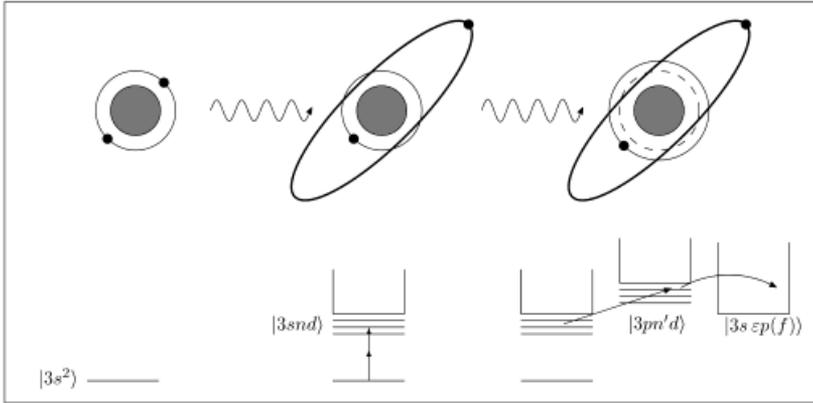
Figure 1: Example of an isolated core excitation process in Mg. After the atom has been prepared in a $|3snd\rangle$ Rydberg state a further laser pulse excites the core $3s - 3p$ transition. In the excited core channel autoionization is possible.

excited channel. The extent of shakeup, i.e. the amount of change in principal quantum number, depends on how strongly the alteration of the core potential is felt by the Rydberg electron. A quantitative measure for this is given by the difference in quantum defects of the two series involved. It has to be noted that the excited channel has autoionizing character as it lies far above the first ionization threshold.

The above discussion suggests to describe isolated core excitation processes by an interaction operator of the form

$$V_{\text{ICE}} = -\frac{1}{2}\,\Omega_{21}(|\Phi_2\rangle\,\langle\Phi_1| + |\Phi_1\rangle\,\langle\Phi_2|) \otimes \mathbf{1}_r \tag{1}$$

from which the role of the Rydberg electron as a spectator becomes obvious. In Eq. (1), $\mathbf{1}_r$ denotes the identity operator for the radial coordinate r of the Rydberg electron, and the $|\Phi_i\rangle$ are the channel wave functions of the two Rydberg series involved. These channel wave functions include the state of the ionic core as well as spin and angular momentum of the Rydberg electron [1, 2]. The Rabi frequency of the core transition is given by $\Omega_{21} = \langle\Phi_2|\,\boldsymbol{d}\cdot\boldsymbol{e}\,|\Phi_1\rangle\,\mathscr{E}$ and is assumed to be real-valued. Thereby, $\boldsymbol{d}$ denotes the atomic dipole operator and $\mathscr{E}$, $\boldsymbol{e}$ are the electric field amplitude and polarisation, respectively. From Eq. (1) it follows that the angular momentum of the Rydberg electrons is conserved in an ICE transition. As the two channels have opposite parity, there is no configuration interaction between them. Despite its simplicity the ansatz (1) describes actual ICE processes to a very high degree of accuracy as many experimental and theoretical studies have shown [18].

Weak field isolated core excitations: So far, investigations involving isolated core excitations have mostly been performed in the perturbative regime where the core transition is driven by a weak laser field. Typically, one studies the frequency dependence of the transition rate for excitation of the autoionizing channel 2 from an initially prepared Rydberg state in channel 1. Thereby, valuable information about the details of the shakeup process is obtained. According to Fermi's golden rule the transition rate is given by the expression $\Gamma(\omega) = 2\pi\,|\langle n_1|\,\langle\Phi_1|\,V_{\text{ICE}}\,|F_\varepsilon\rangle|^2$ with the laser frequency ω, the initial state $|n_1\rangle\,|\Phi_1\rangle$ of energy ε_1 and the excited state $|F_\varepsilon\rangle$ of energy $\varepsilon = \varepsilon_1 + \omega$ (we use Hartree atomic units with "$\hbar = e = m_e = 1$"). With the help of Eq. (1) and methods of multi-channel quantum

defect theory (MQDT) [2, 3] the determination of the rate is reduced to the calculation of the overlap integral between Coulomb functions which is discussed below. Finally, one obtains

$$
\Gamma(\omega) = 2\pi \left(\frac{\Omega_{21}}{2}\right)^2 \nu_1^{-3} \frac{\sin^2 \pi(\nu_1 - \nu_2)}{\pi^2(\varepsilon_1 + \omega - \varepsilon)^2} \left(1 - e^{-4\pi \operatorname{Im} \mu_2}\right) \left|e^{-2\pi i \nu_2} - e^{2\pi i \mu_2}\right|^{-2}
$$

$$
\operatorname*{\simeq}_{\operatorname{Im} \mu_2 \ll 1} 2 \left(\frac{\Omega_{21}}{2}\right)^2 \nu_1^{-3} \frac{\sin^2 \pi(\nu_1 - \nu_2)}{(\varepsilon_1 + \omega - \varepsilon)^2} \frac{\operatorname{Im} \mu_2}{|\sin \pi(\nu_2 + \mu_2)|^2} \tag{2}
$$

with the complex quantum defect μ_2 of channel 2 and the effective quantum numbers ν_i of initial and final state. Thus, the transition rate is essentially given by the product of the square of the overlap integral $\sin \pi(\nu_1 - \nu_2)/(\pi(\varepsilon_1 + \omega - \varepsilon))$ of the radial Rydberg wave functions and the density of states $|e^{-2\pi i \nu_2} - e^{2\pi i \mu_2}|^{-2}$ of the autoionizing Rydberg states in channel 2. Due to their coupling to the continuum channel these states acquire a finite spectral width leading to an ionization rate of $2 \operatorname{Im} \mu_2/\nu_2^3$ and an ionization probability of $4\pi \operatorname{Im} \mu_2$ per round trip of the Rydberg electron around the nucleus. In case the real parts of the quantum defects of the two channels are equal the energy dependence of overlap integral and density of states implies that only the Rydberg state with $n_2 = n_1$ is excited in channel 2 (Fig. 2(a)). The effect of the ICE transition on the Rydberg electron and thus the shakeup are minimal in this case as the scattering phase is not changed by the excitation. However, in case the quantum defects differ from each other a larger number of Rydberg
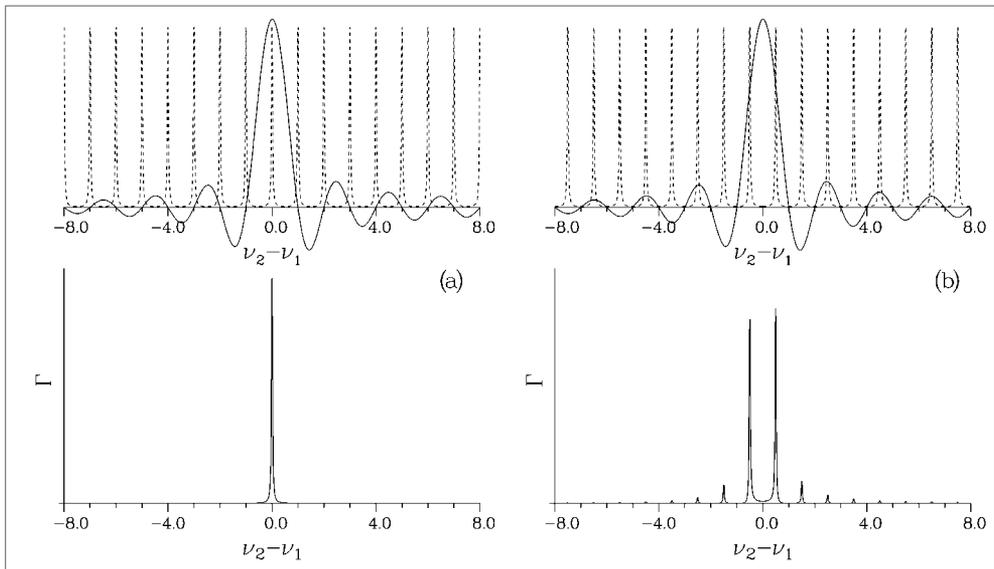

Figure 2: Dependence of the transition rate on the difference in quantum defects. The upper figures show the overlap integral of the radial wave functions $\sin \pi(\nu_2 - \nu_2)/(\pi(\varepsilon + \omega - \varepsilon_1))$ (full curves) and the density of states $|e^{-2\pi i \nu_2} - e^{2\pi i \mu_2}|^{-2}$ (dashed) as a function of $\nu_2 - \nu_1$ for fixed $\nu_1 = 50$, $\mu_1 = 0.0$ and $\mu_2 = 0.0 + i \cdot 0.02$ (a), $\mu_2 = 0.5 + i \cdot 0.02$ (b). In the first case one maximum of the density of states coincides with the central maximum of the overlap integral whereas the other maxima lie in its zeroes: the transition rate Γ therefore displays a single maximum as shown in the lower figure. In the other case the maxima of the density of states coincide with the local extrema of the overlap integral or lie in the sides of the central maximum: several states are excited.

states in channel 2 may be excited which all have a nonvanishing overlap integral with the initial state (Fig. 2(b)).

The overlap integral for Coulomb functions: The overlap integral between Coulomb functions plays an important role in the theory of isolated core excitations. In the calculation of the transition rate $\Gamma(\omega)$ of Eq. (2), for example, it is brought into play in the following way: Describing the ICE interaction in the form of Eq. (1) the determination of $\Gamma(\omega)$ is reduced to the evaluation of the overlap intergral of radial Rydberg wave functions. This integral may be split up into two parts corresponding to the radial coordinate r being smaller or larger than the ionic core radius r_e, respectively. The core radius is of the order of a few Bohr radii whereas the entire Rydberg wave function extends over a region with a radius of about $3n^2/2$ Bohr radii. Therefore, the inner integration which would have to be performed numerically gives only a small contribution which may be neglected to a very good degree of approximation. Outside the core region the radial dependence of the wav functions may be described in the framework of MQDT with the help of Coloumb functions. In the present case one obtains $\langle r \,|\, n_1 \rangle \,|\Phi_1\rangle = \frac{i}{2}(-1)^{l+1}\,\nu_1^{-3/2}\mathscr{C}_l(r;\,\varepsilon_1)\,|\Phi_1\rangle$ and $\langle r \,|\, F_e \rangle = i\mathscr{C}_l(r;\,\varepsilon)\,e^{-i\pi\nu_2}(e^{-2\pi i\nu_2} - \chi_{22})^{-1}\,\chi_{23}\,|\Phi_2\rangle + F_3(r;\,\varepsilon)\,|\Phi_3\rangle$ for $r \geq r_e$. For the following it is convenient to introduce Coulomb functions $\mathscr{C}_l(r\,\varepsilon)$ of energy ε and angular momentum l which are defined by

$$\mathscr{C}_l(\varepsilon;\,r) = \phi_l^-(\varepsilon;\,r)\,e^{i\pi\nu} - \phi_l^+(\varepsilon;\,r)\,e^{-i\pi\nu} \tag{3}$$

with the incoming and outgoing Coulomb functions $\phi_l^\pm$ as given in [1]. The functions $\mathscr{C}_l$ converage to zero for $r \to \infty$ for all complex ε except for ε real and positive. The symmetric unitary scattering matrix χ characterizes the configuration interaction between the channels involved. In the present case it is a 3×3-matrix with $\chi_{31} = \chi_{32} = 0$. The radial wave function $F_3(r)$ in the continuum channel needs not to be specified further in the present context.

The essential problem thus consists in the calculation of $\int_{r_c}^\infty dr\,\mathscr{C}_l(r;\,\varepsilon_2)\,\mathscr{C}_l(r;\,\varepsilon_1)$. Consider first the case of both ε_i complex, but not real and positive. The starting point for the evaluation according to Ref. [28] are the identities $\mathscr{C}_l(\varepsilon_i)\,(\varepsilon_j - h)\,\mathscr{C}_l(\varepsilon_j) = 0$ with $(i, j) = (1, 2)$ and $(2, 1)$, respectively. Thereby, h denotes the radial Coulomb operator $-\frac{1}{2}\frac{d^2}{dr^2} + \frac{l(l+1)}{2r^2} - \frac{1}{r}$. Subtracting one of these equations from the other and integrating from r_c to ∞ one obtains after an integration by parts

$$\int_{r_c}^\infty dr\,\mathscr{C}_l(r;\,\varepsilon_2)\,\mathscr{C}_l(r;\,\varepsilon_1) = \frac{W[\mathscr{C}_l(\varepsilon_2),\,\mathscr{C}_l(\varepsilon_1)]_\infty - W[\mathscr{C}_l(\varepsilon_2),\,\mathscr{C}_l(\varepsilon_1)]_{r_c}}{2(\varepsilon_2 - \varepsilon_1)} \tag{4}$$

with $W[f, g]_r$ the Wronskian of f and g at r. As the functions $\mathscr{C}_l$ go to zero for large r, $W[\mathscr{C}_l(\varepsilon_2),\,\mathscr{C}_l(\varepsilon_1)]_\infty$ vanishes. To determine the Wronskian at r_c one makes use of the weak energy dependence of the functions $\phi_l^\pm$ for small r: the relation $W[\phi_l^-(\varepsilon),\,\phi_l^+(\varepsilon)]_r = 4i/\pi$ will hold approximately at $r \approx r_c$ if ϕ_l^- and ϕ_l^+ are taken at two energies with $|\varepsilon_1 - \varepsilon_2| \ll 1$. Using the definition (3) one thus obtains [27]

$$\int_{r_c}^\infty dr\,\mathscr{C}_l(r;\,\varepsilon_2)\,\mathscr{C}_l(r;\,\varepsilon_1) = \frac{4 \sin \pi(\nu_2 - \nu_1)}{\pi(\varepsilon_2 - \varepsilon_1)}\,. \tag{5}$$

As it would have been expected the integral vanishes whenever $|\nu_2 - \nu_1|$ is equal to a positive integer. The overlap integrals may also be evaluated with continuum wave func-

tions. For ε_1 real and positive one obtains

$$\int_{r_c}^{\infty} dr\, \mathscr{C}_l(r;\, \varepsilon_2)\, \phi_l^{(\pm)}(r;\, \varepsilon_1) = -\frac{2ie^{\pm i\pi\nu_1}}{\pi(\varepsilon_1 - \varepsilon_2)}\, . \tag{6}$$

Finally we consider two continuum wave functions $S(\varepsilon_1)$ and $S(\varepsilon_2)$ $(\varepsilon_i > 0)$ which behave asymptotically as $S(\varepsilon_i) \simeq s_l \cos(\pi\mu_i) + c_l \sin(\pi\mu_i)$. Thereby, s_l and c_l denote the real-valued Coulomb functions of Ref. [1]. The overlap integral for these functions is given by

$$\int_{r_c}^{\infty} dr\, S(r;\, \varepsilon_2)\, S(r;\, \varepsilon_1) = \delta(\varepsilon_2 - \varepsilon_1) \cos \pi(\mu_2 - \mu_1)$$

$$+ \mathscr{P}\, \frac{1}{\pi(\varepsilon_2 - \varepsilon_1)} \sin \pi(\mu_2 - \mu_1) \tag{7}$$

with $\mathscr{P}$ denoting the principal value. To derive this expression one has to take into account also the Wronskian $W[S(\varepsilon_2),\, S(\varepsilon_1)]_{\infty}$ which is not vanising in general.

As it was mentioned above the ICE method which was introduced by COOKE et al. in 1978 [12] has found its main application so far in the frequency-resolved study of highly excited autoionizing states in alkaline earth atoms [18]. Its particular advantage stems from the fact that it allows one to excite selectively the doubly excited quasi-bound Rydberg states without simultaneously exciting degenerate continua. In this way the interpretation of optical spectra is greatly facilitated.

However, in recent years one could observe a growing interest in the use of the ICE technique in time-resolved investigations as well as in questions concerning isolated core excitations in the nonperturbative regime. For example, ROBICHEAUX [19] theoretically considered the following problem: two Rydberg series coupled by a continuous laser field through ICE are excited from a low-lying bound state with a weak laser field. It was predicted that nonperturbative modifications in the resulting photoabsorption spectra could be observed experimentally as soon as the Rabi frequency of the core transition exceeds the total resolution of the probe laser-atom system. VAN DRUTEN and MULLER [20, 21] investigated the excitation of an isolated core transition with an intense fs-pulse and with the atom initially prepared in a bound Rydberg state. In their experiment they were able to observe nonperturbative modifications of the ionization spectrum as well as the population of Rydberg states adjacent to the initial one as soon as the maximum induced Rabi frequency larger than the mean orbit frequency of the Rydberg electron.

In the work of WANG and COOKE [22] a perturbative short pulse isolated core excitation is used to prepare an autoionizing Rydberg wave packet. Studying the time evolution of this wave packet they showed that it does not autoionize according to an exponential decay law, but in a sequence of discrete stair steps separated by the orbital period of the wave packet. This is due to the fact that autoionization is mediated by the interaction of the Rydberg electron with the ionic core and can thus only occur if the wave packet is close to the nucleus. It was shown that the effect of stepwise decay may be exploited for the creation of "dark wave packets". A dark wave packet is a spatially localized minimum in the otherwise slowly varying probability density of a Rydberg electron which shows a time development similar to a normal wave packet. STORY, DUNCAN, and GALLAGHER [23] examined experimentally the possibility of exciting the second valence electron in Mg after preparing the first one as a Rydberg wave packet. Contrary to the case of resonant excitation an off-resonant core excitation is only effective when the wave packet is close to the nucleus. This is due to the fact that in this case the photon energy has to

be partitioned between core and Rydberg electron which is only possible if both are close together.

Recently, a mechanism closely related to isolated core excitation was investigated both theoretically and experimentally in a number of articles [24]. In these studies, a particular manifestation of electron correlation effects in the multiphoton ionisation of two-electron atoms was worked out which was termed continuum-continuum Autler-Townes splitting: the authors considered the photoelectron spectrum obtained in a setup in which a short and intense laser pulse excites one electron into the continuum thereby simultaneously driving Rabi oscillations of the other. If this core resonance were not excited one would expect a single maximum in the photoelectron spectrum (neglecting higher-order photon absorptions). However, in the presence of the Rabi-oscillations this maximum splits up into a double-peak structure with a peak separation equal to the effective Rabi frequency. The nature of this effect which is due to electron correlations may readily be explained within the picture of "dressed Rydberg channels" described in the next subsection: one can think of the electron to be simultaneously excited into two fragmentation channels the thresholds of which are separated by the Rabi frequency. Aspects of the multiphoton ionisation of two-electron atoms in which one electron is initially prepared in a Rydberg state are examined in Refs. [25] and [26]. For the case of ionization with a short and intense pulse it is shown that depending on whether the mean orbit time of the Rydberg electron is shorter or longer than the pulse duration preferably the outer or the inner electron is excited into the continuum.

In view of these investigations it is quite natural to ask how the dynamics of a radial Rydberg wave packet is influenced by the interaction with a residual ionic core in which Rabi oscillations are induced by an intense laser field. This question has aroused some interest in the literature recently and it is this particular aspect of laser-induced electron correlation effects in two-electron atoms the present article will focus on. The purpose of this section consists in putting the basics of the problem into perspective, providing an adequate framework for the theoretical description and discussing main features of the coherent wave packet dynamics. Questions of dissipative influences and the connection with the atomic center of mass motion are deferred to the subsequent sections.

2.2.   Theoretical description of ICE processes in intense laser fields

Isolated core excitation processes in intense laser fields are conveniently described within the framework of MQDT. The concept of "dressed Rydberg channels" [19] which later on proves very helpful for a qualitative understanding of various aspects of the wave packet behavior is thus introduced in a natural way. In order to work out the main features of the derivation most clearly in the following we examine an excitation process in a two-channel system (Fig. 3) in which autoionization of the core-excited channel is neglected. However, the discussion may easily be generalized to more complicated N-channel cases.

An alkaline earth atom is initially prepared in a low lying bound state $|g\rangle$ with energy ε_g. The atom is situated in a cw-laser field

$$\boldsymbol{E}(t) = \mathscr{E}\boldsymbol{e}e^{-i\omega t} + \text{c.c.} \tag{8}$$

which is tuned near resonance with a transition of the positively charged ionic core. Typically electron correlations imply that as long as the atom remains in the initial state $|g\rangle$ this laser field is well detuned from any atomic transition. Therefore it has negligible effect on the atomic dynamics. But as soon as an outer atomic valence electron is excited to Rydberg states close to threshold the cw-laser field starts to induce transitions between the two resonantly coupled states of the ionic core which energies ε_1 and ε_2, respectively. In the
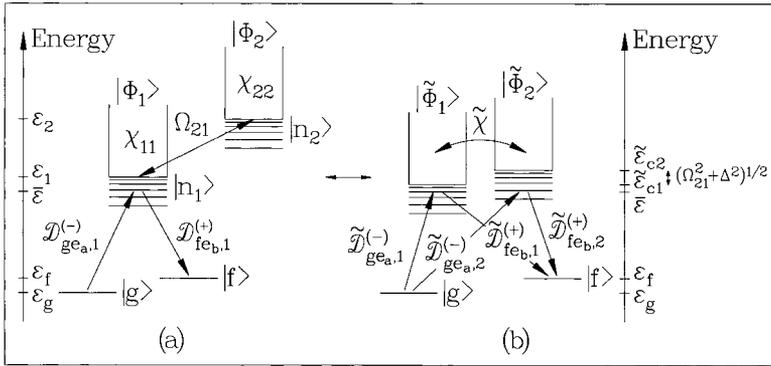
Figure 3: Excitation scheme for the two channel model: (a) bare Rydberg series, (b) "dressed" Rydberg series.

following only intensities I of the laser field $\boldsymbol{E}(t)$ are considered which are small in comparison with the atomic unit, i.e. $I \ll 10^7$ Wcm^{-2}. In this case effects of laser-induced transitions of the excited Rydberg electron to continuum states well above threshold, which could take place in addition to core transitions, are expected to be small and will be neglected in the following. However, they can be incorporated in the formalism easily with the help of intensity dependent quantum defects [15].

In the following we consider the case in which the valence electron is excited coherently to the Rydberg states by a short and weak laser pulse

$$E_a(t) = \mathscr{E}_a(t)\, \boldsymbol{e}_a\, e^{-i\omega_a t} + \text{c.c.},\tag{9}$$

where $\mathscr{E}_a(t)$ is a Gaussian-shaped envelope centered around time t_a with pulse duration τ_a. This implies that a radial electronic Rydberg wave packet is generated by this short laser pulse. The wave packet moves in the Coulomb field of the positively charged ionic core. Whenever it penetrates the core region it is shaken up by the Rabi oscillations of the almost resonantly coupled ionic core states. Effects of this shake-up process on the dynamics of the electronic Rydberg wave packet may be probed, for example, by a second time-delayed short laser pulse (frequency ω_b, polarization $\boldsymbol{e}_b$, pulse duration τ_b) which is centered around time t_b and which induces transitions to an energetically low lying bound atomic state $|f\rangle$ with energy ε_f. Typically this final state does not coincide with the initial state $|g\rangle$. The interaction of the atom with both pulses takes place in a region which extends a few Bohr radii around the atomic nucleus only [1, 15, 39]. Therefore the probability of observing after the interaction with both laser pulses the atomic in the final state is large whenever the initially prepared radial electronic Rydberg wave packet is close to the atomic nucleus. The dependence of the pump-probe signal on the time delay between both pulses thus yields a picture of the wave packet dynamics. For the sake of simplicity let us assume in the following that the envelopes of pump and probe pulse are identical and that $\varepsilon_g + \omega_a = \varepsilon_f + \omega_b = \bar{\varepsilon}$. It should be noted that wave packet detection with the phase-sensitive pump-probe detection scheme [36] which is most frequently used today may also be described within the formalism introduced below. In this case the quantity $|M_{f_g}(t)|^2$ (with $f = g$) has to be interpreted as the variance of the measured Rydberg population after pump and probe pulse. This variance is obtained by altering the delay between both pulses by amounts of the order of several optical cycles.

In the detection scheme mentioned first the probability of observing after the interaction with both laser pulses the atom in state $|f\rangle$ is given by $P_{f_g}(t_b - t_a) = |M_{f_g}(t_b - t_a)|^2$ with [1, 13]

$$M_{f_g}(t_b - t_a) = -\frac{1}{2\pi i} \int\limits_{-\infty + i0}^{\infty + i0} d\varepsilon \, e^{-i\varepsilon(t_b - t_a)} \tilde{\mathscr{E}}_b^*(\varepsilon - \bar{\varepsilon}) \, T_{f_g}(\varepsilon) \, \tilde{\mathscr{E}}_a(\varepsilon - \bar{\varepsilon}) . \tag{10}$$

This expression is valid in lowest order perturbation theory with respect to pump and probe pulse and provided that $|t_b - t_a| \gg \tau_a, \tau_b$. The Fourier transforms of the envelope functions of pump and probe pulse are denoted by

$$\tilde{\mathscr{E}}_k(\varepsilon) = \int\limits_{-\infty}^{\infty} dt \, \mathscr{E}_k(t) \, e^{i\varepsilon(t - t_k)} \tag{11}$$

with $\tilde{\mathscr{E}}_b(\varepsilon) = \tilde{\mathscr{E}}_a(\varepsilon)$ as stated above. The two-photon transition amplitude

$$T_{f_g}(\varepsilon) = \langle f| \, d \cdot e_b^* \, \frac{1}{\varepsilon - H} \, d \cdot e_a \, |g\rangle , \tag{12}$$

with d the atomic dipole operator, describes the response of the atom in the intense cw-laser field $E(t)$ to pump and probe pulse. Thereby, the Hamiltonian operator H characterizes the dynamics in the excited atomic channels under the influence of the intense cw-laser field $E(t)$. In the dipole and rotating wave approximation it is given by

$$H = H_1 + H_2 + V_{\text{ICE}} . \tag{13}$$

The Hamiltonians

$$H_j = (h_{jj} + V_{jj}(r) + \varepsilon_{cj}) \, |\Phi_j\rangle \, \langle\Phi_j| \tag{14}$$

describe the electronic dynamics in the bare atomic channels 1 and 2 in the absence of the cw-laser field. The radial Hamiltonian for the Rydberg electron in channel j with angular momentum l_j is given by $(h_{jj} + V_{jj}(r))$ with $h_{jj} = -\frac{1}{2}\frac{d^2}{dr^2} + \frac{l_j(l_j+1)}{2r^2} - \frac{1}{r}$ and $V_{jj}(r)$ the short-range potential which describes effects of the residual core electrons. Due to the conservation of angular momentum in the ICE transition one has $l_1 = l_2 = l$. The channel thresholds in the RWA are given by $\varepsilon_{c1} = \varepsilon_1$, $\varepsilon_{c2} = \varepsilon_2 - \omega$. The operator V_{ICE} is defined in Eq. (1).

The main problem in the theoretical description of nonperturbative ICE transitions is thus the determination of the two-photon transition amplitude. This goal may be achieved with the help of the Dalgarno-Lewis method [37] by solving the inhomogeneous Schrödinger equation

$$(\varepsilon - H) \, |\lambda(\varepsilon)\rangle = d \cdot e_a \, |g\rangle \tag{15}$$

from which the two-photon transition amplitude is obtained by the relation

$$T_{f_g}(\varepsilon) = \langle f| \, d \cdot e_b^* \, |\lambda(\varepsilon)\rangle . \tag{16}$$

The inhomogeneous Schrödinger equation can be solved with the help of methods MQDT. For this purpose we adopt an ansatz of the form

$$\langle \Omega, r \, | \, \lambda(\varepsilon)\rangle = \sum_{j=1,2} \Phi_j(\Omega) \, F^{(j)}(r; \varepsilon)/r . \tag{17}$$

The channel coordinates Ω represent the coordinates of the core electrons and the angular momentum and spin of the excited Rydberg valence electron. The radial part of the wave function of the excited Rydberg valence electron in channel j is denoted by $F^{(j)}(r;\varepsilon)$. Projection of Eq. (15) onto the normalized channel states $|\Phi_j\rangle$ yields

$$\left\{\varepsilon - \left[\boldsymbol{h} + \boldsymbol{\varepsilon}_c + \boldsymbol{V}(r) - \frac{1}{2}\,\boldsymbol{\Omega}_{21}\right]\right\}\boldsymbol{F}(r;\varepsilon) = \boldsymbol{D}(r). \tag{18}$$

The 2×2 matrices $\boldsymbol{h}$, $\boldsymbol{V}$, $\boldsymbol{\varepsilon}_c$ and $\boldsymbol{\Omega}_{21}$ are obtained in an obvious way from Eqs. (14) and (1). The components of the column vector $\boldsymbol{F}(r;\varepsilon)$ are the radial wave functions of the Rydberg valence electron $F^{(j)}(r;\varepsilon)$. The laser-induced coupling between state $|g\rangle$ and the excited channels is described by the column vector $\boldsymbol{D}(r)$ with matrix elements $D_j(r) = r\int d\Omega\,\Phi_j^*(\Omega)\,\boldsymbol{d}\cdot\boldsymbol{e}_a\langle\Omega, r\,|\,g\rangle$. In the excitation scheme under consideration the coupling between $|g\rangle$ and channel 2 may be neglected $(D_2(r) = 0)$. We can assume $V_j(r) \simeq 0$ and $D_1(r) \simeq 0$ for r greater than the core radius r_c. In the close-coupling equations (18) the laser-induced interaction between both channels appears as a long-range interaction independent of the radial coordinate r of the Rydberg valence electron.

In order to determine the two-photon transition amplitude we subject Eq. (18) to the orthogonal transformation

$$\boldsymbol{O} = \begin{pmatrix} \cos\varphi & -\sin\varphi \\ \sin\varphi & \cos\varphi \end{pmatrix} \tag{19}$$

which is defined by the eigenvalue relation

$$\boldsymbol{O}^T\left(\boldsymbol{\varepsilon}_c - \frac{1}{2}\,\boldsymbol{\Omega}_{21}\right)\boldsymbol{O} = \tilde{\boldsymbol{\varepsilon}}_c. \tag{20}$$

The 2×2 matrix $\boldsymbol{O}$ describes the transformation between the bare core channel states $|\Phi_j\rangle$ and the corresponding photon-dressed core channel states [19]. The diagonal matrix $\tilde{\boldsymbol{\varepsilon}}_c$ defines the dressed energies of the ionic core. Explicitly these dressed energies are given by $(\tilde{\boldsymbol{\varepsilon}}_c)_{11} \equiv \tilde{\varepsilon}_{c1} = \varepsilon_{c1} - \frac{1}{2}\Omega_{21}\tan\varphi$ and $(\tilde{\boldsymbol{\varepsilon}}_c)_{22} \equiv \tilde{\varepsilon}_{c2} = \varepsilon_{c2} + \frac{1}{2}\Omega_{21}\cot\varphi$. The corresponding rotation angle φ is defined by the relation $\tan(2\varphi) = \Omega_{21}/\Delta$ with the detuning $\Delta = \varepsilon_{c2} - \varepsilon_{c1}$. Applying this transformation to the inhomogeneous Schrödinger equation (18) yields

$$\{\varepsilon - [\boldsymbol{h} + \tilde{\boldsymbol{\varepsilon}}_c + \tilde{\boldsymbol{V}}(r)]\}\tilde{\boldsymbol{F}}(r;\varepsilon) = \tilde{\boldsymbol{D}}(r) \tag{21}$$

with the transformed configuration interaction matrix $\tilde{\boldsymbol{V}}(r) = \boldsymbol{O}^T\boldsymbol{V}(r)\,\boldsymbol{O}$. The corresponding transformed state vector of the Rydberg valence electron and the transformed dipole-couplings are given by $\tilde{\boldsymbol{F}}(r;\varepsilon) = \boldsymbol{O}^T\boldsymbol{F}(r;\varepsilon)$ and $\tilde{\boldsymbol{D}}(r) = \boldsymbol{O}^T\boldsymbol{D}(r)$, respectively.

Eq. (21) shows that as far as the dressed channels are concerned the long-range coupling contained in Eq. (18) causes two effects: on the one hand, it leads to an energy shift of the ionization thresholds which is due to the ac-Stark splitting of the dressed ionic core states. This shift — together with the form (31) of the photoionization dipole matrix elements — is also the reason for the appearance of the continuum-continuum Autler-Townes splitting [38]. On the other hand, a short-range coupling is induced between the dressed channels which is described by the transformed configuration interaction $\tilde{\boldsymbol{V}}(r)$. Outside the ionic core, i.e. for $r \geq r_c$, this coupling vanishes and the Rydberg electron dynamics is described by the pure diagonal Coulomb hamiltonian. Eq. (21) is thus of a form amenable to an analysis by the methods of MQDT. In particular, it follows that formally a two-channel Rydberg system with (laser-induced) short-ranged configuration interaction may be asso-

ciated with Eq. (21) (Fig. 3(b)). This Rydberg system is characterized by a 2×2 scattering matrix $\tilde{\chi}$ and, furthermore, by photoionization and -recombination dipole matrix elements $\tilde{\mathscr{D}}_{ge_a}^{(-)}$ and $\tilde{\mathscr{D}}_{fe_b}^{(+)}$ which describe the coupling to the low lying bound states $|g\rangle$ and $|f\rangle$ [4]. These quantities are smooth functions of energy across any threshold [2, 39]. From Refs. [1, 13] it follows that the two-photon transition amplitude for the transformed system which is equal to the transition amplitude for the original one is given by

$$T_{fg}(\varepsilon) = T_{fg}^{(s)} + 2\pi i \tilde{\mathscr{D}}_{fe_b}^{(+)} (e^{-2\pi i \tilde{\nu}} - \tilde{\chi})^{-1} \, \tilde{\mathscr{D}}_{ge_a}^{(-)} . \tag{22}$$

The diagonal 2×2 matrix $e^{-2\pi i \tilde{\nu}}$ has elements

$$(e^{-2\pi i \tilde{\nu}})_{jj} = \exp\left\{-2\pi i [2(\tilde{\varepsilon}_{cj} - \varepsilon)]^{-1/2}\right\} . \tag{23}$$

The smooth part of the transition amplitude can be partitioned into $T_{fg}^{(s)} = T_{fg,nr}^{(s)} + i\pi \tilde{\mathscr{D}}_{fe_b}^{(+)} \tilde{\chi}^* \tilde{\mathscr{D}}_{ge_a}^{(-)}$. It can be shown that the non-resonant part $T_{fg,nr}^{(s)}$ does not enter into actual calculations of M_{fg} [34].

It remains to determine the analytical form of the dressed scattering matrix $\tilde{\chi}$ and the dressed energy-normalized dipole matrix elements. For this purpose we consider the homogeneous Schrödinger equation in the absence of the intense cw-laser field, i.e.

$$\{\varepsilon - [h + \varepsilon_c + V(r)]\} \, \mathscr{F}^{(+)}(r; \varepsilon) = 0 . \tag{24}$$

As $V_{12}(r) = V_{21}(r) \equiv 0$ this equation has a 2×2 fundamental system of energy-normalized regular solutions of the form

$$\mathscr{F}^{(+)}(r; \varepsilon) = \frac{1}{2} \left[\boldsymbol{\phi}^-(r; \varepsilon) - \boldsymbol{\phi}^+(r; \varepsilon)\, \boldsymbol{\chi}\right] \quad \text{for} \quad r \geq r_c \tag{25}$$

with

$$\boldsymbol{\chi} = \begin{pmatrix} e^{2\pi i \mu_1} & 0 \\ 0 & e^{2\pi i \mu_2} \end{pmatrix} \tag{26}$$

and $\mathscr{F}_{12}^{(+)}(r; \varepsilon) = \mathscr{F}_{21}^{(+)}(r; \varepsilon) = 0$ for $0 \leq r < \infty$. The quantum defects of the undressed Rydberg series are given by μ_j and $\boldsymbol{\phi}^\pm(\varepsilon)$ denote the 2×2 diagonal matrices of incoming and outgoing Coulomb functions $[\boldsymbol{\phi}^\pm(\varepsilon)]_{jj} = \phi^\pm(\varepsilon - \varepsilon_{cj})$.

Following the arguments of Robicheaux [19] in terms of these solutions an approximate fundamental system of regular solutions of the homogeneous part of Eq. (21) for the energy region above both thresholds is given by

$$\tilde{\mathscr{F}}_{jk}^{(+)}(r; \varepsilon) = \sum_{i,l=1,2} O_{ji}^T \mathscr{F}_{il}^{(+)}(r; \varepsilon + \varepsilon_{ci} - \tilde{\varepsilon}_{cj}) \, O_{lk} \tag{27}$$

with $\tilde{\mathscr{F}}_{jk}^{(+)}$ the j-th vector component of the k-th solution $(j, k = 1, 2)$. The insertion of this ansatz into the left hand side of Eqs. (21) yields

$$(\varepsilon - h_{jj} - \tilde{\varepsilon}_{cj}) \, \tilde{\mathscr{F}}_{jk}^{(+)}(r; \varepsilon) - \sum_{m=1,2} \tilde{V}(r)_{jm} \tilde{\mathscr{F}}_{mk}^{(+)}(r; \varepsilon)$$

$$= \sum_{l,m,n,p=1}^{2} O_{jm}^T [V(r)\, O]_{ml} \, O_{ln}^T [\mathscr{F}_{np}^{(+)}(r; \varepsilon + \varepsilon_{cm} - \tilde{\varepsilon}_{cj}) - \mathscr{F}_{np}^{(+)}(r; \varepsilon + \varepsilon_{cn} - \tilde{\varepsilon}_{cl})] \, O_{pk} . \tag{28}$$

Thereby, one takes into account that the angular momenta of the Rydberg electron in both channels coincide. For $r > r_c$ the right hand side of Eq. (28) vanishes because outside the core region the core potentials $V(r)$ vanish. For $r \leq r_c$ the difference between the solutions $\mathscr{F}_{np}^{(+)}(r; \, \varepsilon + \varepsilon_{cm} - \tilde{\varepsilon}_{cj})$ and $\mathscr{F}_{np}^{(+)}(r; \, \varepsilon + \varepsilon_{cn} - \tilde{\varepsilon}_{cl})$ can be estimated semiclassically to be of the order of $(r_c^{3/2} \max \{|\Delta|, |\Omega_{21}|\})$ [39]. For typical core radii of a few Bohr radii and laser intensities I much less than the atomic unit of intensity, i.e. $I \ll 10^{17}$ Wcm^{-2}, this difference is thus vanishingly small. On the other hand, the short-range potentials behave as $V_{ij}(r) \simeq -(Z - 1) \, \delta_{ij}/r + a_{ij} + o(1)$ for small r with Z the nuclear charge and a_{ij} constants of the order of the atomic unit. However, a short calculation shows that the divergent contributions $-(Z - 1) \, \delta_{ij}/r$ compensate so that the right hand side of Eq. (28) is everywhere small. Therefore, to a good degree of approximation a fundamental system of regular solutions of the homogeneous part of Eq. (21) is given by Eq. (27).

The functions $\mathscr{F}^{(+)}$ behave asymptotically as

$$\tilde{\mathscr{F}}_{jk}^{(+)}(r; \, \varepsilon) \simeq \delta_{jk}\phi_l^-(r; \, \varepsilon - \tilde{\varepsilon}_{cj}) + \phi_l^+(r; \, \varepsilon - \tilde{\varepsilon}_{cj}) \, \tilde{\boldsymbol{\chi}}_{jk} \,. \tag{29}$$

with

$$\tilde{\boldsymbol{\chi}} = \boldsymbol{O}^T \boldsymbol{\chi} \boldsymbol{O} \,. \tag{30}$$

Eq. (30) thus yields the dressed scattering matrix. From the definition of the photoionization dipole matrix elements $\mathscr{D}^{(-)} = -\tilde{\boldsymbol{\chi}} \int_0^\infty dr \, \mathscr{F}^{(+)\dagger}(r) \, \boldsymbol{D}(r)$ it follows that

$$\tilde{\mathscr{D}}_{ge_a}^{(-)} = \boldsymbol{O}^T \tilde{\mathscr{D}}_{ge_a}^{(-)} \tag{31}$$

and, correspondingly,

$$\tilde{\mathscr{D}}_{fe_b}^{(+)} = \mathscr{D}_{fe_b}^{(+)} \boldsymbol{O} \,. \tag{32}$$

In the particular excitation scheme of Fig. 3 the 2-components of the bare dipole matrix elements are equal to zero. Inserting Eqs. (30)–(32) into Eq. (22) yields the final expression for the two-photon transition amplitude. The validity of this result may also be checked numerically [29].

Eqs. (30)−(32) show that the laser-induced coupling of the bare core states is transferred in a simple way to the Rydberg channels: the dressed eigenstates of the core are obtained from the bare ones by the orthogonal transformation $(\Phi_1, \, \Phi_2) \, \boldsymbol{O} = (\tilde{\Phi}_1, \, \tilde{\Phi}_2)$. This connection is conveyed directly to the scattering matrix and the dipole matrix elements. By an appropriate choice of the parameters which characterize this laser-induced coupling, i.e. detuning Δ and Rabi frequency Ω_{21}, "unusual" scattering matrices which have large off-diagonal elements may be realized. This aspect is further investigated in the following subsection. A second effect of the laser-induced coupling consists in shifting the energies of the channel thresholds to the values of the dressed core states. These shifts are taken into account in the diagonal matrix $e^{-2\pi i \tilde{\nu}}$.

Perturbative theoretical descriptions of ICE transitions are recovered in the limit $|\varphi| \approx |\Omega_{21}/2\Delta| \ll 1$ [19, 29]. For example, assume that the core-excited Rydberg series is slightly coupled to a continuum channel and consider the following typical situation from energy-resolved spectroscopy: A first weak cw-laser with amplitude $\mathscr{E}_1$ and frequency ω_1 excites the initial state $|g\rangle$ almost resonantly to a Rydberg state $|n_1\rangle$ in channel 1. A second weak cw-laser couples $|n_1\rangle$ to states $|\nu_2\rangle$ in the autoionizing channel 2 with energies $\varepsilon_{\nu_2} = \varepsilon_2 - 1/(2\nu_2^2)$. Modeling the autoionizing character of the Rydberg series in channel 2 by a complex quantum defect μ_2 the depletion rate Γ of the initial state $|g\rangle$ is given by

$\Gamma = -2 |\mathcal{E}_1|^2 \operatorname{Im} T_{gg}(\varepsilon_g + \omega_1)$ according to Fermi's Golden rule. For this quantity one obtains from Eq. (22) in the limit $|\varphi| \approx |\Omega_{21}/2\Delta| \ll 1$ and $\operatorname{Im} \mu_2 \ll 1$

$$
\Gamma = \left\{ \frac{2\pi^2 (\Omega_1/2)^2}{\sin^2 \pi(\nu_1 + \mu_1)} \right\} \left\{ \left(\frac{\Omega_{21}}{2} \right)^2 \frac{\operatorname{Im} \mu_2}{|\sin \pi(\nu_2 + \mu_2)|^2} \frac{\sin^2 \pi(\nu_1 - \nu_2)}{\Delta^2} \right\}, \qquad (33)
$$

with the Rabi frequency of the transition $|g\rangle \to |n_1\rangle$ denoted by Ω_1. Thereby the effective quantum number ν_1 is related to the excited energy in channel 1 by $\varepsilon_g + \omega_1 = \varepsilon_1 - 1/(2\nu_1^2)$. In Eq. (33) the first term in curly brackets can be interpreted as the probability of (almost resonant) excitation of the bound Rydberg state $|n_1\rangle$ from the initial state $|g\rangle$. The second term describes one-photon excitation of the autoionizing channel states $|\nu_2\rangle$ from the bound Rydberg state $|n_1\rangle$ in accordance with Eq. (2).

It should be noted that the above description may easily be generalized to multichannel transition processes in which the initial state is excited into a group of Coulomb fragmentation (free) channels which may be coupled to further free channels by electron correlations and by laser-induced excitations of the ionic core [19, 29]. Thereby the laser-induced excitations of the core can arise from one or several cw-laser fields. In particular, Eqs. (22) and (30)−(32) remain valid if the matrix O is interpreted as the transformation matrix between the bare and dressed core states in the N-channel system. Another extension of the formalism concerning wave packet preparation by power broadening is described in Ref. [29]. In this case the ICE-coupled Rydberg series are excited from the initial state by an intense cw-laser field. A wave packet will be generated if the state $|g\rangle$ is depleted on a time scale short in comparison with the mean wave packet orbit time [15].

2.3.   Electronic Rydberg wave packet dynamics under the influence of laser-induced core transitions

In this subsection the theoretical results derived above are used to examine various aspects of the dynamics of electronic Rydberg wave packets under the influence of isolated core excitations. In the first part the technique of semiclassical path expansions is used to discuss how the effects of electron correlations and laser-field intensity are reflected in the short-time behavior of the pump-probe signal. Subsequently a kind of synchronization between wave packet and core dynamics is described which is obtained by choosing the wave packet orbit time equal to an integer multiple of the core Rabi period [30]. In this way the autoionization of the Rydberg electron is effectively inhibited. Finally it is shown that the investigation of the dressed eigenenergies of the atom in the laser field yields an alternative approach to the qualitative understanding of the wave packet dynamics.

2.3.1.   Short-time behavior of the pump-probe signal

In order to work out the effects of laser-induced core excitation on the wave packet dynamics most clearly we consider in the following again the excitation scheme of Fig. 3 in which autoionization may formally be taken into account with the help of complex quantum defects. These ICE effects are conveniently analyzed by representing the pump-probe probability in the form of a semiclassical path expansion [1]. For this purpose we insert expression (22) into Eq. (10) and expand the inverse matrix as a geometric series. Thus the probability of observing the atom in state $|f\rangle$ after the interaction with both short laser

pulses is given by

$$
P_{fg}(t_b - t_a)
$$

$$
= \left| \int\limits_{-\infty + i0}^{\infty + i0} d\varepsilon \, e^{-i\varepsilon(t_b - t_a)} \, \tilde{\mathscr{E}}_a^*(\varepsilon - \bar{\varepsilon}) \, \tilde{\mathscr{D}}_{fe_b}^{(+)} \sum_{M=1}^{\infty} \left(e^{2\pi i \tilde{\nu}} - \tilde{\boldsymbol{\chi}} \right)^{M-1} e^{2\pi i \tilde{\nu}} \, \tilde{\mathscr{D}}_{ge_a}^{(-)} \tilde{\mathscr{E}}_a(\varepsilon - \bar{\varepsilon}) \right|^2
$$

$$(34)$$

as long as $|t_b - t_a| \gg \tau_a, \tau_b$.

Eq. (34) conveys the following picture for the wave packet evolution: after the initial short pulse excitation (characterized by the photoionization amplitudes $\tilde{\mathscr{D}}_{ge_a}^{(-)}$ only those fractions of the radial electronic Rydberg wave packet which are excited into closed dressed channels will return again to the core region and therefore contribute to $P_{fg}(t_b - t_a)$. On each complete orbital round trip such a fraction acquires a phase of $e^{2\pi i \tilde{\nu}_{jj}}$. Thereby, the quantity $2\pi \tilde{\nu}_{jj}$ is the classical action which a Rydberg electron of energy $(\varepsilon - \tilde{\varepsilon}_{ci}) < 0$ accumulates during one period of motion along a purely radial Kepler orbit with zero angular momentum. Each time a fraction of the radial electronic Rydberg wave packet returns to the core region it may be scattered into the other dressed channel. This scattering process is described by the dressed scattering matrix $\tilde{\boldsymbol{\chi}}$. If autoionization is present the moduli of the eigenvalues of $\tilde{\boldsymbol{\chi}}$ are less than 1 so that at every scattering event some parts of the wave function are lost into the continuum. The action of the probe pulse is characterized by the factor $\tilde{\mathscr{E}}_a^*(\varepsilon - \bar{\varepsilon}) \, \tilde{\mathscr{D}}_{fe_b}^{(+)}$. According to this interpretation of Eq. (34) the M-th summand of the series describes the contribution to the pump-probe signal which is associated with the M-th return of the excited Rydberg electron to the core region.

In the dressed channel picture the effect of the cw-laser field on the wave packet dynamics is thus described by the modification of the quantities $\tilde{\boldsymbol{\chi}}$, $\tilde{\mathscr{D}}_{ge_a}^{(-)}$ and $\tilde{\mathscr{D}}_{fe_b}^{(+)}$ on the one hand and by the shift of the thresholds $\tilde{\varepsilon}_{c,i}$ on the other hand. Therefore, the most important parameters which determine the behavior of the wave packet are (1) the ratio between the Rabi period $T_{\mathrm{Rabi}} = 2\pi/\Omega_{21}$ of the ionic core and the wave packet orbit time T_{orb} and (2) the difference of the quantum defects of the bare Rydberg series which determines the extent of the shakeup. The associated effects become manifest already in the short-time behavior of the pump-probe signal (i.e. for pump-probe delays of the order of several orbit times) and are exhibited in the following for two extreme cases. Thereby, wave packets are considered with a mean excited quantum number of $\bar{\nu}_1 = [2(\tilde{\varepsilon}_{c1} - \bar{\varepsilon})]^{-1/2} = 80$, i.e. $T_{\mathrm{orb}} = 2\pi \bar{\nu}_1^3 = 77.8$ ps, the laser field is tuned to the core resonance ($\Delta = 0$, $\varphi = \pi/4$), and autoionization is neglected. The envelopes of the pump and probe pulses are given by $\mathscr{E}_a(t) = \mathscr{E}_a^{(0)} \exp\left(-4(\ln 2)\,(t - t_{a(b)})^2/\tau^2\right)$ with a pulse length of $\tau = 0.3 T_{\mathrm{orb}}$. Further examples are discussed in Refs. [29] and [34].

(a) Weak core excitation ($T_{\mathrm{Rabi}} \ll T_{\mathrm{orb}}$) *and minimum shakeup* ($\mu_2 - \mu_1 = 0.0$): For equal quantum defects of the bare Rydberg series the dressed scattering matrix $\tilde{\boldsymbol{\chi}}$ is a multiple of the unit matrix. This implies that after the initial excitation which occurs with equal amplitude into both dressed channels the two fractions of the prepared wave packet are not scattered by the laser-excited core but remain in their respective dressed channel in the course of the time evolution. Furthermore, if the core excitation is weak the dressed thresholds are only slightly shifted so that the two wave packet fractions have almost equal orbit times and return to the core simultaneously. However, the slight energy shift leads to a difference in the phases which the wave packet fractions accumulate during one complete round trip around the nucleus. It is approximately equal to $\Delta S = T_{\mathrm{orb}} |\Omega_{21}|$. Therefore, even a weak core excitation is clearly manifest in the pump-probe signal in the form of interference effects: the phase difference leads to a modulation of the magnitude of the recurrence
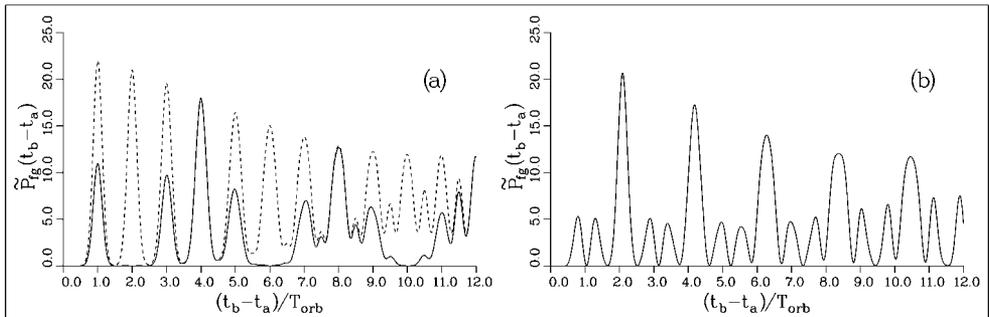
Figure 4: Scaled pump-probe probability $\tilde{P}_{fg} = P_{fg}/|\mathscr{D}^{(+)}_{feb,1}\mathscr{D}^{(-)}_{gea,1}\tilde{\mathscr{E}}^{(0)2}_{a}\tau|^2$ as a function of the time delay $t_b - t_a$ (in units of T_{orb}) for (a) $\mu_1 = \mu_1 = 0.0$, $T_{Rabi} = 4T_{orb}$, and (b) $\mu_1 = 0.0$, $\mu_1 = 0.5$, $T_{Rabi} = 0.081T_{orb}$. The other parameter values are $\Delta = 0$, $\bar{\nu}_1 = 80$, $T_{orb} = 77.8$ ps and $\tau = 0.3T_{orb}$. The dashed curve in Fig. 4(a) shows the pump-probe signal in the absence of laser-induced core coupling ($\Omega_{21} = 0$).

peaks in the pump-probe probability with an envelope function approximately given by $\cos^2\left[|\Omega_{21}|(t_2 - t_1)\right]$. These modulations reflect the Rabi oscillations of the ionic core: whenever the core is in (bare) state 2 or 1 the overlap between the Rydberg wave packet and state $|f\rangle$ (and therefore the pump-probe probability) vanishes or is maximal. This behavior is exemplified in Fig. 4(a) for the case of $T_{Rabi} = 4T_{orb}$. For the sake of comparison the dashed curve shows the time evolution of $P_{(fg)}(t_b - t_a)$ in the absence of laser-induced core transitions, i.e. for $\Omega_{21} = 0$.

(a) Strong core excitation ($T_{Rabi} \ll T_{orb}$) and maximum shakeup ($\mu_2 - \mu_1 = 0.5$): For $\mu_2 - \mu_1 = 0.5$ the dressed scattering matrix is given by

$$\tilde{\chi} = e^{2\pi i\mu_1}e^{i\pi}\begin{pmatrix} 0 & 1 \\ 1 & 0 \end{pmatrix}.$$

Therefore the shakeup of the Rydberg electron caused by the laser-induced core transitions is so effective that at each return to the core region the two fractions of the electronic Rydberg wave packet which evolve in the dressed channels are scattered from one channel into the other with a probability of unity. This scattering mechanism is clearly visible in Fig. 4(b) in which a case of strong laser-induced core coupling with $T_{Rabi} = 0.081T_{orb}$ is shown. Such a Rabi period implies a larger separation of the thresholds of the dressed channels and thus a significant difference in the orbit times of the wave packet fractions which are prepared initially in the dressed channels. At odd multiples of T_{orb}, e.g. at the first return, two-peaked maxima are observed which represent the temporally separated returns of the two fractions. However, at each return to the region the faster part of the wave packet is scattered into the dressed channel with the longer return time and vice versa. Therefore at even multiples of T_{orb} both fractions reach the core simultaneously and their contributions to the pump-probe probability add constructively giving rise to one-peaked large maxima.

For an intermediate difference in quantum defects the wave packet is split up into a rapidly growing number of fractions in the course of its successive returns to the nucleus. This is due to the fact that in this case both diagonal and off-diagonal elements of the dressed scattering matrix are non-vanishing. For weak core excitations the semiclassical path representation is still useful to predict the relative heights of the successive recurrence peaks in the pump-probe signal in an simple way [34]. For stronger excitations the behavior of the pump-probe signal is conveniently discussed with the help of other methods which are discussed subsequently.

A few remarks should be made as to the experimental realization of the discussed pump-probe scheme and the observability of the effects described so far. A real alkaline earth atom constitutes a complicated multi-channel system. However, it is possible to realize to a good degree of approximation a two-channel system with respect to the ICE transition by performing all excitations with circularly polarized light and making use of the selection rules for angular momentum [21, 40]. Couplings to further channels then arise only through configuration interactions which can be taken into account in the present context by a complex quantum defect μ_2. Typical values for $\mathrm{Im}\,\mu_2$ lie in the range between 10^{-3} and 10^{-1} [41]. Numerical calculations show that for $\mathrm{Im}\,\mu_2 \leq 0.01$ only minor quantitative modifications in the short-time behavior of the pump-probe signal appear while the characteristic qualitative features are left unchanged [29].

Differences in quantum defects actually observed for ICE transitions lie in the whole range between 0.0 and 0.5 (e.g., the transition Sr $5snd \rightarrow 5p_{1/2}nd$ comes rather close to 0.5 [12]). As the value of the core dipole matrix is typically of the order of 1 au one expects laser intensities of about $10\,\mathrm{kW/cm^2}$ to drive the core transition with $T_{\mathrm{orb}} = T_{\mathrm{Rabi}}$ for $\bar{\nu}_1 = 80$. This intensity scales with $\bar{\nu}_1^{-6}$. The relevant wavelengths lie in the range between 250 and 450 nm. It suggests itself to realize the core transition with a ns-pulse which is switched on before pump pulse arrives and switched off after the probe pulse. Pulses of this kind which reach the necessary intensity without being too tightly focussed may be produced nowadays. In view of this discussion the observation of the described effects should be feasible with presently available means. Work in this direction is already in progress [42].

2.3.2. Synchronization of wave packet and core dynamics

If one synchronizes the dynamics of the ionic core and the wave packet a long-time stabilization of the Rydberg electron against autoionization can be achieved. This effect may be understood as follows: when the wave packet is excited by the short laser pulse the core is essentially in the ground state $|\Phi_1\rangle$. If the wave packet orbit time is chosen equal to a multiple of the Rabi period of the core the Rydberg electron will encounter a de-excited core at each of its returns to the nucleus. Therefore, the wave packet is scattered from the excited core (i.e. core state $|\Phi_2\rangle$) only to a very small extent, the effects of shakeup and autoionization are thus minimal and the wave packet behaves as if it would propagate in a single-channel system with a de-excited core [19]. Hanson and Lambropoulos [30] worked out the significance of this effect for the creation of slowly autoinizing non-dispersing wave packets. Dispersion is inhibited because the Rabi-oscillating core works as a quantum-mechanical shutter which effectively cuts off the tails of the wave packet which arrive at the nucleus out of phase.

Formally, this stabilization effect is explained within the framework of Sec. 2.2 as follows [19]: one considers the time-independent transition amplitude $T_{fg}(\varepsilon)$ in the vicinity of energies ε_m for which $\tilde{\nu}_{11}(\varepsilon_m) - \tilde{\nu}_{22}(\varepsilon_m) = m$ with $m \in \mathbf{Z}$. To a good degree of aproximation this condition is equivalent to $T_{\mathrm{orb}} = |m|\,T_{\mathrm{Rabi}}$. For energies ε with $\varepsilon - \varepsilon_m \ll |\varepsilon - \varepsilon_{m\pm1}|$ it follows that $e^{2\pi i \hat{\nu}} \simeq e^{2\pi i \hat{\nu}}\mathbf{1} \equiv e^{2\pi i \hat{\nu}}$ with $\hat{\nu} = [2(\hat{\varepsilon} - \varepsilon)]^{-1/2}$. Thereby, one can choose $\hat{\varepsilon} = \tilde{\varepsilon}_{c1}$ or $\hat{\varepsilon} = \tilde{\varepsilon}_{c2}$. Inserting this approximation for $e^{2\pi i \hat{\nu}}$ into the expression for T_{fg} one obtains

$$T_{fg}(\varepsilon) \simeq T_{fg}^{(2)} + 2\pi i \tilde{\mathscr{D}}_{fe_b}^{(+)}(e^{-2\pi i \hat{\nu}} - \boldsymbol{\chi})^{-1}\tilde{\mathscr{D}}_{ge_a}^{(-)}. \tag{35}$$

This expression is (apart from the substutution of the bare channel thresholds by $\hat{\varepsilon}$) identical to the transition amplitude for the system in the absence of ICE-Coupling with the wave packet excited in the $|\Phi_1\rangle$-channel.
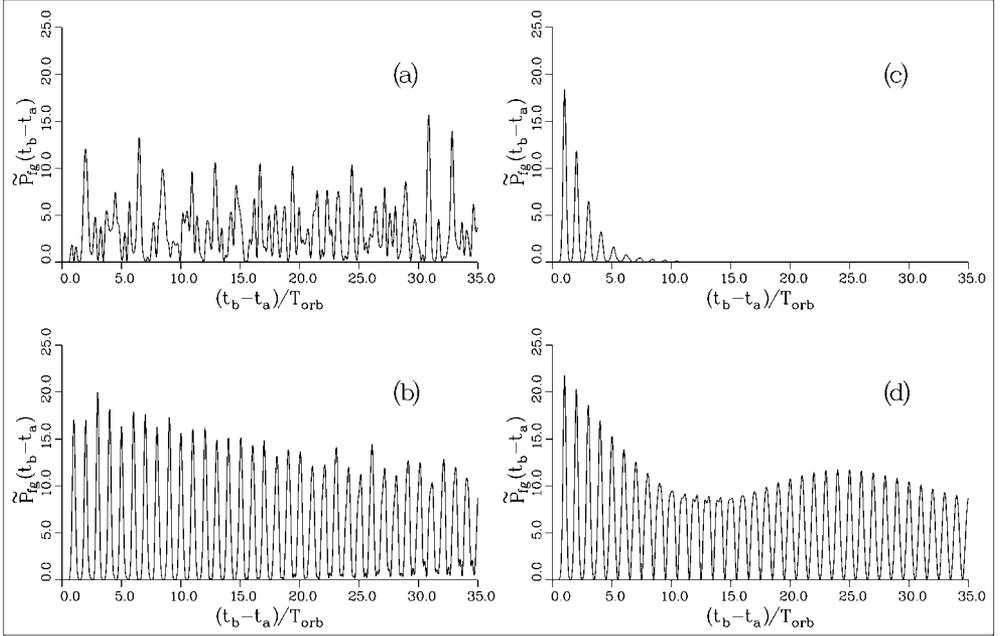
Figure 5: Synchronization of core wave packet dynamics. Parameter values of Figs. (a) and (b): $\mu_1 = 0.0$, $\mu_2 = 0.25$, $\Omega_{21} = 7.81 \cdot 10^{-6}$ au, $\Delta = 0$, $\tau = 23.3$ ps, and $\bar{\nu}_1 = 83$ (a), $\bar{\nu}_1 = 80$ (b), i.e. $T_{orb} = 4.47 T_{Rabi}$ (a), $T_{orb} = 4.0 T_{Rabi}$ (b). Parameter values of Figs. (c) and (d): $\mu_1 = 0.0$, $\mu_2 = 0.0 + i0.1$, $\bar{\nu}_1 = 80$, Δ and τ as above, and $\Omega_{21} = 1.70 \times 10^{-6}$ au ($T_{orb} = 0.87 T_{Rabi}$) (c), $\Omega_{21} = 1.95 \cdot 10^{-6}$ au ($T_{orb} = 1.0 T_{Rabi}$) (d).

In Fig. 5 two examples for this effect are depicted. In Figs. 5(a), (b) two pump-probe signals are compared for a non-autoionizing two-channel system with intermediate shakeup $(\mu_2 - \mu 1 = 0.25)$ and fixed Rabi frequency, but different mean excited energies $\bar{\varepsilon}$. In Fig. 5(b), where $T_{orb} = 4 T_{Rabi}$ was chosen, the pump-probe signal shows a very regular behavior which is typically observed in one-channel systems. Shifting $\bar{\varepsilon}$ such that $T_{orb} = 4.5 T_{Rabi}$ the signal acquires   an appearance which looks very complicated at first sight but which is amenable to further analysis within the dressed energy approach. In Figs. 5(c), (d) the influence on the wave packet autoionization is illustrated which was worked out in Ref. [30]. In the figures a two-channel system with $\mu_1 = 0.0$ and $\mu_2 = 0.0 + i0.1$ is considered. For $T_{orb} = 0.87 T_{orb}$ (Fig. 5(c)) the dynamics of core and wave packet are not synchronized, the wave packet also encounters the core in the excited state at its returns to the nucleus and therefore autoionizes very rapidly. If the intensity is changed such that $T_{orb} = T_{Rabi}$ autoionization is effectively suppressed.

2.3.3.   Dressed state energies and wave packet dynamics

The method os semiclassical path expansion is particularly useful to obtain a qualitative understanding of the wave packet dynamics in the short-time domain, i.e. for times up to several multiples of T_{orb} where the number of relevant recurrence contributions is sufficiently low. An alternative approach is provided by studying the behavior of the eigenenergies $\tilde{\varepsilon}_n$ of the dressed states, i.e. the solutions to the equation
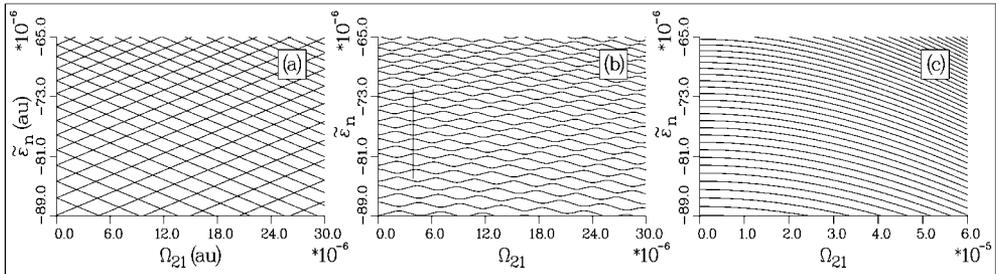
$$\det \left(e^{-2\pi i \tilde{\nu}} - \tilde{\chi} \right) = 0 . \tag{36}$$

Figure 6: Eigenenergies of dressed Rydberg states (relative to the "bare" threshold ε_{c1}) as a function of Ω_{21} for resonant coupling $\Delta = 0$ and (a) $\mu_1 = \mu_2 = 0.0$, (b) $\mu_1 = 0.0$, $\mu_2 = 0.25$, (c) $\mu_1 = 0.0$, $\mu_2 = 0.5$. The vertical line in (b) indicates the energy region with $\Omega_{21} = 3.91 \cdot 10^{-6}$ au and $\tilde{\nu}_{11}(\varepsilon) - \tilde{\nu}_{22}(\varepsilon) \simeq 2$ which is examined more closely in Fig. 7.

In Fig. 6 these dressed energies are shown as a function of the laser-induced core coupling strength Φ_{21} for various differences of the quantum defects μ_1 and μ_2 and resonant laser-induced core coupling $\Delta = 0$.

Fig. 6(a) displays the case $\mu_1 = \mu_2$. This spectrum can be under-stood within the picture of two independent dressed channels which was also used for the discussion of the wave packet dynamics pertaining to this case (cf. Fig. 4(a)). The dressed eigenstates are given by $|\tilde{n}\rangle |\tilde{\Phi}_{1(2)}\rangle = 2^{-1/2}(|n\rangle |\Phi_1\rangle \pm |n\rangle |\Phi_2\rangle)$ and can thus be assigned unambiguously to one of the dressed channels. Their eigenenergies $\tilde{\varepsilon} = -1/2(n - \mu_1)^2 \pm \frac{1}{2}\Omega_{21}$ exhibit directly the ac-Stark splitting of the core states. The spectrum is therefore divided into two groups of linearly ascending and descending energy levels which intersect each other without avoided crossings. At the crossing points the difference $\tilde{\nu}_{11}(\varepsilon) - \tilde{\nu}_{22}(\varepsilon)$ is an integer. Fig. 6(a) thus shows from another point of view that the excitation by a short laser pulse leads two the creation of two wave packet fractions which evolve independently from each other and which have different orbit times if Ω_{21} is large enough.

For a difference in quantum defects of $\mu_2 - \mu_1 = 0.25$ (Fig. 6(b)) the main feature of the preceding diagram, namely the two groups of linearly ascending and descending energy levels, is still clearly recognizable. However, due to the channel mixing which is caused by the radiative core coupling the energy levels show well-pronounced avoided crossing. The aforementioned main feature of the first two diagrams vanishes completely if the difference in quantum defects is increased to $\mu_2 - \mu_1 = 0.5$ (Fig. 6(c)). In this case the interaction between the dressed channels becomes so strong that the individual eigenstates cannot be assigned to one of the dressed channels. For $\Omega_{21} = 0$ each state has approximately equal distance in energy to both its neighbours. Due to the level repulsion it tends to keep this maximum separation to both sides also when the coupling strength Ω_{21} is increased. This explains the almost horizontal direction of the curves for small values of Ω_{21}. For large enough values of Ω_{21}, however, all levels are gradually pushed downwards because they must always stay below the lower threshold of the Rydberg series which has energy $\varepsilon_{c1} - \frac{1}{2}|\Omega_{21}|$. Fig. 6(c) also gives an alternative explanation for the dynamical behavior shown in Fig. 4(b). As neighboring levels are separated by $1/2 \cdot 1/\nu^3$, approximately, an electronic Rydberg wave packet should regain its initial shape at multiples of $2 \times T_{\text{orb}}$. This explains the well pronounced recurrence peaks which appear at even multiples of T_{orb} in Fig. 4(b).

To explain the synchronization effect of Sec. 2.3.2 within the dressed states approach, in Fig. 7(a) the moduli $|c_{\tilde{n}}|$ of the residues of the two-photon amplitudes $T_{fg}(\varepsilon)$ are depicted for the case $\mu_2 - \mu_1 = 0.25$ and $\Omega_{21} = 3.91 \cdot 10^{-6}$ au. These residues essentially determine the amplitudes for excitation of the dressed states by the short laser pulse. If the mean
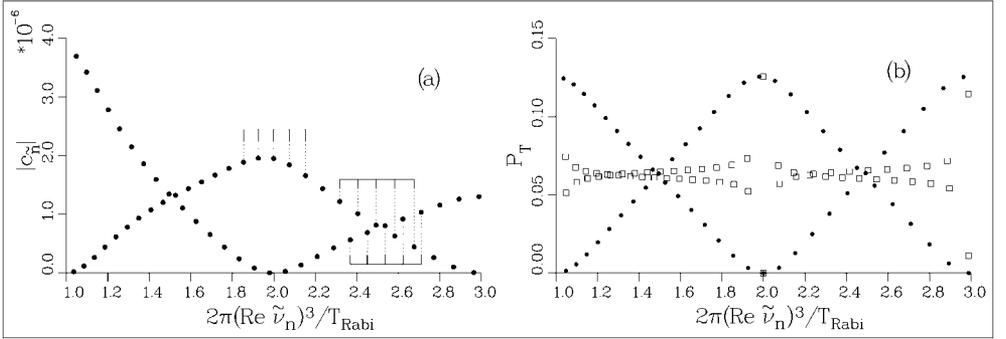
Figure 7: (a): Moduli $|c_{\tilde{n}}|$ of the residues of $T_{fg}(\varepsilon)$ for $\mu_1 = 0.0$, $\mu_2 = 0.25$, $\Delta = 0$, and $\Omega_{21} = 3.91 \cdot 10^{-6}$ as a function of the ratio between wave packet orbit time $2\pi(\mathrm{Re}\,\tilde{\nu}_n)^3$ and the Rabi period. The quantities $|c_{\tilde{n}}|$ give a measure for the excitation probabilities of the dressed states. In the vicinity of an avoided crossing (e.g. $T_{orb} = 2T_{Rabi}$) only approximately equidistant states are excited which is indicated by the uppermost "comb". Far from the avoided crossing two "one-channel like" wave packets are excited (the "teeth" of each comb are separated nearly equidistantly; however, this distance differs for the two combs). (b): Autoionization rates per orbit $P_T = -2(\mathrm{Im}\,\tilde{\varepsilon}_n)\,2\pi(\mathrm{Re}\,\tilde{\nu}_n)^3$ for $\mu_2 = 0.25 + i0.01$ ($\bullet$) and $\mu_2 = 0.0 + i0.01$ ($\square$).

excited quantum number $\bar{\nu}_1$ is chosen such that the condition synchronization $T_{orb} = |m|\,T_{Rabi}$ is fulfilled the eigenstates possess either predominantly $|\Phi_1\rangle$ or $|\Phi_2\rangle$ character, i.e. either large or small excitation probability. The states with large excitation probability are separated nearly equidistantly by an amount of $\bar{\nu}_1^{-3}$ so that the excited wave packet behaves in a way similar to the one-channel case. For eigenenergies with $\tilde{\nu}_{11}(\tilde{\varepsilon}_n) - \tilde{\nu}_{22}(\tilde{\varepsilon}_n) \simeq m + \frac{1}{2}$ which are far away from the avoided crossings the spectrum displays a behavior similar to a system with equal quantum defects (cf. Fig. 6(b)). Thus, the individual eigenstates may approximately be assigned to a particular dressed channel. Correspondingly, all these states have nearly the same excitation probability. This means that an excitation in this region essentially creates two independently evolving wave packet fractions similar to the case without shakeup. Pump-probe signals like the one of Fig. 6(c) may therefore be thought of as arising from the interference of the contributions of the two fractions. The behavior of each of these contributions is regular as in the one-channel case.

Furthermore, it is unteresting to study the behavior of the autoionization rates of the dressed eigenstates which is depicted in Fig. 7(b) for a case with parameters identical to Fig. 7(a) except that now $\mathrm{Im}\,\mu_2 = 0.01$. Away from the avoided crossings the states have approximately equal autoionization rates. In the vicinity of the crossings the weakly excited states carry nearly the whole probability of ionization as they have $|\Phi_2\rangle$ character. The strongly excited states ionize slowly. This splitting appears also in the case $\mathrm{Re}\,(\mu_2 - \mu_1) = 0.0$ but is less pronounced [20].

3.   Spontaneous Emission of Photons by Isolated-core Excited Two-electron Atoms

In this section it is investigation how ICE processes are influenced by radiative damping of the laser-excited ionic core. Spontaneous emission of photons by the ionic core tends to destroy quantum coherences of an electronic Rydberg wave packet via electron correlation effects. Vice versa the dynamics of an electronic Rydberg wave packet may also influence the process of photon emission by the tightly bound core electron. So far in the context of wave packet dynamics in Rydberg systems the problem of destruction of quantum coher-

ence by dissipative and stochastic influences has not received much attention. To a large extent this might be traced back to the fact that due to the high level density of Rydberg systems the solution of the relevant master equations constitutes a difficult mathematical and numerical problem. The purpose of the subsequent section is twofold, namely

(1) to obtain physical insight into the intricate interplay between laser-modified electron correlation effects, the spontaneous emission of photons by a laser-excited ionic core and the semiclassical aspects of the dynamics of an excited Rydberg electron and

(2) to present an adequate theoretical approach which is capable of dealing with the difficulties arising from the description of dissipative phenomena in Rydberg systems close to a photoionization threshold.

It will be demonstrated that a decomposition of the relevant master equation into N-photon contributions and the application of semiclassical path representations yield a practical and physically transparent theoretical description. In the context of laser-induced stabilization against autoionization, which has been studied in detail in Sect. 2.3.2, it will be shown that the destruction of quantum coherence by radiative damping of the ionic core may lead to significant physical effects. This may hyppen even in cases in which characteristic autoionization rates are much larger than radiative decay rates of the ionic core. Finally, the influence of the dynamics of an electronic Rydberg wave packet on the process of photon emission by the ionic core is investigated. For this purpose the time dependence of the intensity correlation function of the spontaneously emitted photons is investigated [43].

3.1.   Optical Bloch equations and semiclassical N-photon transition amplitudes

In order to put the problem into perspective let us consider a typical laser-induced two-electron excitation process as shown in Fig. 8 schematically. An electronic Rydberg wave packet is prepared by a short and weak laser pulse $E_a(t)$. Simultaneously the ionic core is excited almost resonantly by a cw-laser field $E(t)$. The dynamics of the electronic Rydberg wave packet under the influence of the Rabi oscillations of the ionic can be investigated for example by a pump-probe type setup as discussed in detail in Sec. 2.2. A major difference to the case already discussed in Sec. 2.2 (compare with Fig. 3) is the possibility of spontaneous emission of photons by the laser-excited ionic core. Effects of autoionization originating from the excited core channel are taken into account by a third (open) continuum channel as indicated in Fig. 8.

For the theoretical description of this ICE process in the presence of radiative damping of the ionic core the master equation

$$\dot{\varrho}(t) = -i[H, \varrho(t)] + \frac{1}{2}\{[L, \varrho(t) L^\dagger] + [L\varrho(t), L^\dagger]\} \tag{37}$$

has to be solved for the reduced density operator of the laser-excited atom. Thereby the initially unoccupied modes of the radiation field, into which a photon can be emitted spontaneously by the ionic core, have been traced out [44]. The Hamiltonian H describes the coherent part of the atomic two-electron excitation process and is defined by the corresponding three-channel generalization of Eqs. (1), (13) and (14). The stochastic part of the atomic dynamics is described by the Lindblad operator

$$L = \sqrt{\varkappa}\,|\Phi_1\rangle\,\langle\Phi_2| \tag{38}$$

which characterizes the radiative decay of the ionic core from state $|\Phi_2\rangle$ to state $|\Phi_1\rangle$ by spontaneous emission of photons with rate $\varkappa$. Due to the very long lifetimes of Rydberg states radiative decay of the excited Rydberg electron can be neglected.

A straightforward way of solving the optical Bloch equation (37) numerically is obtained by expanding the density operator $\varrho(t)$ into a basis set of operators constructed from the energy eigenfunctions. However, this approach is only feasible as long as the number of significantly contributing energy eigenstates is sufficiently small. In particular, severe problems arise in cases in which Rydberg states are excited directly at the ionization threshold. An alternative theoretical approach for solving this master equation was proposed originally by MOLLOW [44]. It is based on a representation of the density operator in terms of a (fictitious) ensemble of pure states which are associated with definite numbers of spontaneously emitted photons. The dynamics of these pure states can be determined with the help of semiclassical methods which have already proven useful for the dynamical description of Rydberg electrons and their threshold phenomena. Such a semiclassical pure state approach yields direct physical insight into the classical aspects of the dynamics of Rydberg electrons and the destruction of quantum coherence which is caused by the radiative decay of the ionic core. From a practical point of view this theoretical approach is expected to be particularly useful in cases in which the number of spontaneously emitted photons is small. Furthermore, this way all effects arising from the infinitely many Rydberg states converging to the ionization threshold and the adjacent electron continua can be taken into account properly.

The starting point for MOLLOW's approach [44] is the decomposition of the reduced atomic density operator of Eq. (37) into contributions which are associated with the spontaneous emission of exactly photons, i.e.

$$\varrho(t) = \sum_{N=0}^{\infty} \varrho^{(N)}(t) \,. \tag{39}$$

The N-photon contribution $\varrho^{(n)}(t)$ can be represented as a mixture of pure N-photon states, i.e.

$$\varrho^{(N)}(t) = \int_0^t dt_N \int_0^{t_N} dt_{N-1} \ldots \int_0^{t_2} dt_1 \, |\psi(t\,|\,t_N, \ldots, t_1)\rangle \, \langle\psi(t\,|\,t_N, \ldots, t_1)| \,. \tag{40}$$

These N-photon states $|\psi(t\,|\,t_N, \ldots, t_1)\rangle$ are determined by (random) jump times $t_1 \leq t_2 \leq \ldots \leq t_N \leq t$. Their time evolution is given by

$$|\psi(t\,|\,t_N, \ldots, t_1)\rangle = e^{-iH_{\mathrm{eff}}(t - t_N)} \theta(t - t_N) \, L e^{-iH_{\mathrm{eff}}(t_N - t_{N-1})} \theta(t_N - t_{N-1}) \, L$$
$$\ldots L e^{-iH_{\mathrm{eff}} t_1} \theta(t_1) \, |\psi(t=0)\rangle \tag{41}$$

with the effective (non-Hermitian) Hamiltonian

$$H_{\mathrm{eff}} = H - \frac{i}{2} L^\dagger L \,. \tag{42}$$

This decomposition of the atomic density operator significant advantages in cases in which the number of spontaneously emitted photons is small or the evaluation of the relevant pure states be simplified by the application of semiclassical methods, for example. In particular, for the master equation (37) it is possible to derive semiclassical path representations for the N-photon pure states $|\psi(t\,|\,t_N, \ldots, t_1)\rangle$ [31]. This way it is possible to express all physical observables of interest as a sum of probability amplitudes which are associated with repeated returns of a Rydberg electron to the ionic core. During its motion under the influence of the Coulomb potential of the ionic core photons may be emitted spontaneously by the laser-excited core at any position of the Rydberg electron along its classical path. These
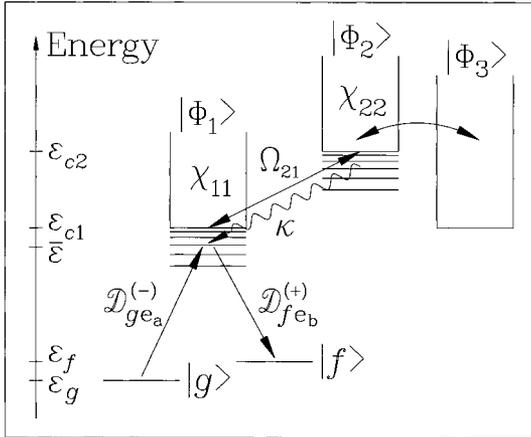
Figure 8: Three-channel excitation scheme including spontaneous emission processes and autoionization.

photon emission processes disrupt the coherent quantum mechanical time evolution of the Rydberg electron.

In order to clarify these ideas let us consider a pump-probe experiment of the type shown in Fig. 8 which has already been discussed in Sec. 2.2 in the absence of radiation damping of the ionic core. From the master equation (37) it can be shown [31] that the pump-probe transition probability in the presence of radiative damping of the ionic core is given by

$$P_{fg}(t_b - t_a) = \sum_{N=0}^{\infty} \int_0^{t_b - t_a} dt_N \int_0^{t_N} dt_{N-1} \ldots \int_0^{t_2} dt_1 \, |A_{gf}^{(N)}(t_b - t_a \,|\, t_N, \ldots, t_1)|^2 \,. \tag{43}$$

Thereby $A_{gf}^{(N)}(t_b - t_a \,|\, t_N, \ldots, t_1)$ denotes the conditional probability amplitude of observing the electronic Rydberg wave packet in final state $|f\rangle$ after the time delay $(t_b - t_a)$ provided the ionic core has emitted exactly N photons spontaneously at times $t_1 \leq t_2 \leq \ldots \leq t_N$. Similar to Eq. (10) the time dependent N-photon transition amplitudes $A_{gf}^{(N)}(\,|\, t_N, \ldots, t_1)$ can be related to associated time-independent N-photon transition amplitudes $T_{fg}^{(N)}(\varepsilon_{N+1}, \ldots, \varepsilon_1)$ by

$$A_{gf}^{(N)}(t \,|\, t_N, \ldots, t_1) = \left(\frac{1}{2\pi} \right)^{N+1} \int_{-\infty + i0}^{\infty + i0} d\varepsilon_{N+1} \ldots \int_{-\infty + i0}^{\infty + i0} d\varepsilon_1 \, e^{-i\varepsilon_{N+1}(t - t_N) - \ldots - i\varepsilon_1 t_1}$$
$$\times \, \tilde{\mathscr{E}}_b^*(\varepsilon_{N+1} - \bar{\varepsilon}) \, T_{fg}^{(N)}(\varepsilon_{N+1}, \ldots, \varepsilon_1) \, \tilde{\mathscr{E}}_a(\varepsilon_1 - \bar{\varepsilon}) \,. \tag{44}$$

The zero-photon amplitude $T_{fg}^{(0)}(\varepsilon_1)$ is defineed by Eq. (22). However, in view of the non-Hermitian effective Hamiltonian of Eq. (42) the (bare) threshold energy of the excited channel ε_{c2} becomes complex according to the replacement $\varepsilon_{c2} \to \varepsilon_{c2} - i\varkappa/2$. This has to be taken into account in the definition (20) of the transformation matrix $\boldsymbol{O}$ and the thresholds of the dressed channels. The time-independent one-photon amplitude is given by

$$T_{fg}^{(1)}(\varepsilon_2, \varepsilon_1) = 2\pi i \tilde{\mathscr{D}}_{fe_b}^{(+)} \sum_{M_2 = 0}^{\infty} \sum_{M_1 = 0}^{\infty} (e^{2\pi i \tilde{\nu}_2} \tilde{\chi})^{M_2} \, \tilde{\boldsymbol{S}}_{2,1} (\tilde{\chi} e^{2\pi i \tilde{\nu}_1})^{M_1} \tilde{\mathscr{D}}_{ge_a}^{(-)} \tag{45}$$

with

$$\tilde{\boldsymbol{S}}_{2,1} = \int_0^T d\tau \, e^{2\pi i \tilde{v}_2 (1 - \tau/T)} \left(e^{-i\pi/2} \tilde{\boldsymbol{L}} \right) e^{2\pi i \tilde{v}_1 \tau/T} \tag{46}$$

and $T = (t_b - t_a)/(M_2 + M_1 + 1)$.

The one-photon amplitude of Eq. (45) can be interpreted physically in a straightforward way: After the initial excitation by the short laser pulse which is characterized by the dipole matrix elements $\mathscr{D}_{ge_a}^{(-)}$ those fractions of the electronic Rydberg wave packet which are excited into closed photon-dressed channels perform repeated orbital round trips around the nucleus. On each complete round trip in one of the photon-dressed channels j the Rydberg electron acquires a phase of magnitude $(2\pi \tilde{v}_1)_{jj}$. The quantity $(2\pi \tilde{v}_1)_{jj}$ is equal to the classical action of motion along a purely radial Kepler orbit with zero angular momentum and energy $\varepsilon - \tilde{\varepsilon}_{cj} < 0$. At each return to the ionic core the Rydberg electron can be scattered into other dressed channels by laser-modified electron correlation effects which are characterized by the scattering matrix $\tilde{\chi}$ of Eq. (30). However, during any of the orbital round trips of the Rydberg electron the ionic core can emit a photon spontaneously. The associated probability amplitude is described by the quantity $\tilde{\boldsymbol{S}}_{2,1}$. According to Eq. (46) the photon emission by the ionic core may take place at any time τ with $0 \le \tau \le T$ between two successive returns of the Rydberg electron to the core. At time τ the Rydberg electron has acquired a phase of magnitude $(2\pi \tilde{v}_1 \tau/T)$. The disruption of quantum coherence by the spontaneous emission process is described by the action of the Lindblad operator $\tilde{\boldsymbol{L}} = \boldsymbol{O}^T \boldsymbol{L} \boldsymbol{O}$. In addition, this photon emission is accompanied by a phase change of magnitude $(-\pi/2)$. After the photon emission process the Rydberg electron accumulates an additional phase of magnitude $[(2\pi \tilde{v}_2 (1 - \tau/T)]$ during its subsequent return to the core. As the photon emission process can take place at any time between two successive returns of the Rydberg electron to the core the amplitudes associated with all possible values of the effective photon emission time τ have to be added coherently as described by Eq. (46).

Semiclassical path representations analogous to Eq. (45) can be derived for all N-photon transition amplitudes with $N \ge 2$ [31]. However, thereby it has to be taken into account that during a round trip of the Rydberg electron around the nucleus an arbitrary number of photons n with $0 \le n \le N$ can be emitted spontaneously by the ionic core.

3.2.   Stabilization against autoionization and radiative decay of the ionic core

In a typical ICE process as shown in Fig. 8 the mean autoionization rate of the excited Rydberg electron is given by $\Gamma_{\bar{v}} = 2 \, \text{Im} \, \mu_2/\bar{v}^3$. Therefore, as long as the Rydberg electron is not excited very close to threshold and its angular momentum is not too large its autoionization rate $\Gamma_{\bar{v}}$ is typically much larger than the radiative damping rate of the core transition $\varkappa$. Under these circumstances the influence of radiative damping of the ionic core is usually negligible. Thus, typical pump-probe experiments are described to a very good degree of approximation by the corresponding zero-photon transition amplitude because the atom will autoionize with high probability before the first spontaneous photon can be emitted by the ionic core.

Nevertheless, under certain circumstances the dynamics of an electronic Rydberg wave packet can be affected by the radiative decay of the ionic core considerably. In particular, the coherent mechanism of stabilization against autoionization which has been proposed originally by Hanson and Lambropoulos [30] and which has been discussed in Sec. 2.3.2 is expected to be sensitive against the destruction of quantum coherence which is brought about by spontaneous emission of photons by the ionic core. Laser-induced stabilization against autoionization is achieved by synchronizing the (mean) period of the laser-prepared

electronic Rydberg wave packet T_{orb} with the Rabi-period of the resonantly driven core transition T_{Rabi}, i.e., T_{orb} has to be equal to an integer multiple of T_{Rabi}. Thus, provided the electronic Rydberg wave packet is prepared initially in channel 1, i.e., with the core in its ground state $|\Phi_1\rangle$, with each of its returns to atomic nucleus it will find the ionic core in its ground state $|\Phi_1\rangle$. As autoionization of a Rydberg electron can take place only inside the core region [2, 3] this implies that the effective autoionization rate of the excited Rydberg wave packet will become much smaller than $\Gamma_{\bar{\nu}}$ (compare with Fig. 5(d)). However, in the presence of radiative decay of the ionic core this physical picture is changed completely. In the simplest case of synchronization, i.e. for $T_{orb} = T_{Rabi}$, the first photon will be emitted spontaneously by the ionic core most probably at a time $(m + 1/2) T_{Rab}$, $m \in N$, when the electronic Rydberg wave packet is close to the outer turning point of its classical Kepler orbit. The spontaneous emission of a photon reduces the excited core to its ground state $|\Phi_1\rangle$. Therefore, at the subsequent returns of the electronic Rydberg wave packet to the atomic nucleus at times $(m + n) T_{orb}$, $n \in N$, the ionic core will be in its excited state so that the Rydberg electron will autoionize on a time scale of the order of $1/\Gamma_{\bar{\nu}}$. Thus, the laser-induced stabilization against autoionization will be destroyed. Typically $\Gamma_{\bar{\nu}} \gg \varkappa$ so that the Rydberg electron will autoionize with high probability long before the core can emit a second photon spontaneously. Consequently, it is expected that the influence of the radiative damping on this coherent stabilization phenomenon can be described approximately by taking into account only the zero- and one-photon amplitudes of the relevant transition amplitudes.

In Fig. 9(a) the pump-probe transition probability of the ICE process of Fig. 8 is shown as a function of the time delay between pump- and probe pulses (full curves). The parameters chosen are: $T_{orb} = T_{Rabi}$, $\mu_1 = 0.0$, $\mu_2 = 0.051 + i0.1$, $\varkappa T_{orb} = 0.1$, $\bar{\nu}_1 = 136$. Initially the electronic Rydberg wave packet is prepared by a short laser pulse in channel 1. The dotted and dashed curves depict the zero- and one-photon contributions. The full curve has been evaluated by solving the corresponding optical Bloch equations (37) numerically in the energy representation. The decay of the pump-probe signal on a time scale of the order of $1/\varkappa$ as well as the quality of approximating the pump-probe signal by its zero- and one-photon contributions are apparent. For the sake of comparison Fig. 9(b) shows the pump-probe signal and the zero- and one-photon contributions in the absence of autoionisa-
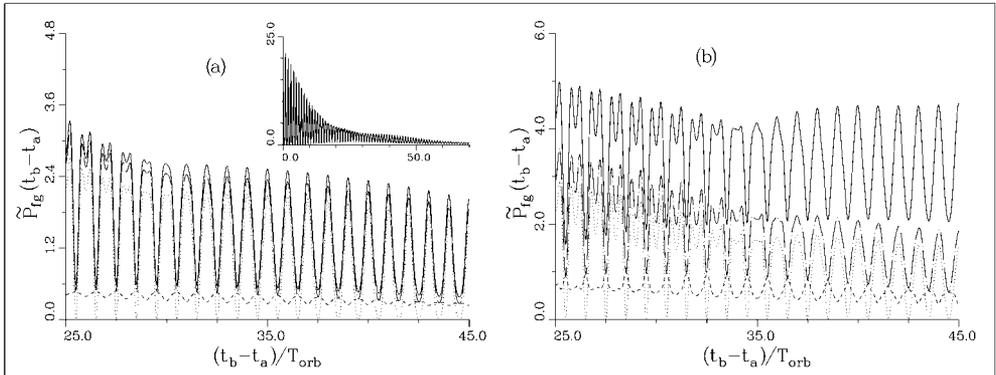

Figure 9: Wave packet evolution under the condition of period matching of orbit time and Rabi period in the presence of spontaneous emission: Scaled pump-probe signal $\tilde{P}_{fg} = P_{fg}/|\mathscr{D}_{fe_b}^{(+)} \mathscr{E}_b^{(0)} \mathscr{D}_{ge_a}^{(-)} \mathscr{E}_a^{(0)} \tau|^2$ (full curve) and contributions $\tilde{P}_{fg}^{(N)}$, $N = 0$ (dotted), 1 (dashed), for $T_{Rabi} = T_{orb}$, $\varkappa T_{orb} = 1/10$, $\bar{\nu}_1 = 136 (T_{orb} = 382 \text{ ps})$, $\Delta = 0$, $\tau = 0.3 T_{orb}$ and $\mu_1 = 0.0$, $\mu_2 = 0.051 + i0.1$ (a); $\mu_2 = 0.051 + i \cdot 0.0$ (b). The chain-dashed curve shows the sum $\tilde{P}_{fg}^{(0)} + \tilde{P}_{fg}^{(1)}$. The inset in Fig. 9(b) displays the global decay of the pump-probe signal on a time scale approximately given by $1/\varkappa$.

tion. It is apparent that in this case photon contributions with higher values of N become relevant soon.

From the experimental point of view it might be difficult to observe the influence of radiative damping of the core transition on laser-induced stabilization against autoionization in a pump-probe experiment. As typically $1/\varkappa \gg T_{\mathrm{orb}}$ the decrease of the pump-probe signal can be observed only for sufficiently long observation times. Furthermore, over these long time scales also other experimental disturbances might lead to a decrease of the pump-probe signal. However, it is expected that the effective time dependent ionization rate $\gamma(t)$, which is close to zero in the absence of spontaneous emission of photons by the ionic core, should be much more sensitive to the decohering effects of radiative damping of the core. An experimental technique for measuring the time dependence of ionization rates has been developed recently by LANKHUIJZEN and NOORDAM [45].

For the three-channel problem shown in Fig. 8 the time-dependent autoionization rate $\gamma(t)$ can be decomposed into its N-photon contributions with the help of the theoretical methods discussed in Sec. 3.1, i.e.

$$\gamma(t) = \sum_{N=0}^{\infty} \int_0^t dt_N \ldots \int_0^{t_2} dt_1 \, \gamma^{(N)}(t \,|\, t_N, \ldots, t_1) \,. \tag{47}$$

Using the notation of Sec. 2 the corresponding zero- and one-photon contributions are given by [31]

$$\gamma^{(0)}(t) = \frac{1}{2\pi} \left(1 - e^{-4\pi \,\mathrm{Im}\,\mu_2}\right)$$
$$\times \left| \int_{-\infty+i0}^{\infty+i0} d\varepsilon_1 \, e^{-i\varepsilon_1 t}(0,\,1,\,0)\, \boldsymbol{O}(\mathbf{1} - e^{2\pi i \bar{\nu}_2}\tilde{\boldsymbol{\chi}})^{-1}\, e^{2\pi i \bar{\nu}_1}\, \tilde{\mathscr{D}}_{ge_a}^{(-)}\tilde{\mathscr{E}}_a(\varepsilon_1 - \bar{\varepsilon}) \right|^2 ,$$
$$\tag{48}$$

$$\gamma^{(1)}(t \,|\, t_1) = \left(\frac{1}{2\pi}\right)^3 \left(1 - e^{-4\pi \,\mathrm{Im}\,\mu_2}\right) \left| \int_{-\infty+i0}^{\infty+i0} d\varepsilon_1 \, d\varepsilon_1 \, e^{-i\varepsilon_2(t-t_1)-i\varepsilon_1 t_1} \right.$$
$$\left. \times (0,\,1,\,0)\, \boldsymbol{O}(\mathbf{1} - e^{2\pi i \bar{\nu}_2}\tilde{\boldsymbol{\chi}})^{-1}\, \tilde{S}_{2,1}(\mathbf{1} - \tilde{\boldsymbol{\chi}} e^{2\pi i \bar{\nu}_1})^{-1}\, \tilde{\mathscr{D}}_{ge_a}^{(-)}\tilde{\mathscr{E}}_a(\varepsilon_1 - \bar{\varepsilon}) \right|^2 .$$

These quantities are very similar to the zero- and one-photon amplitudes of the pump-probe transitions probability discussed in Sec. 3.1. The only major difference is the replacement of $\tilde{\mathscr{D}}_{fe_b}^{(+)}\tilde{\mathscr{E}}_b(\varepsilon_2 - \bar{\varepsilon})$ by $(0,\,1,\,0)\,\boldsymbol{O}$ reflecting the fact that no probe pulse is applied to the atom and that it is only channel 2 which can autoionize. In Eqs. (48) the bare scattering matrix is given by

$$\tilde{\boldsymbol{\chi}} = \begin{pmatrix} e^{2i\pi\mu_1} & 0 & 0 \\ 0 & e^{2i\pi\mu_2} & \chi_{23} \\ 0 & \chi_{32} & \chi_{33} \end{pmatrix} . \tag{49}$$

Furthermore, in Eq. (48) it is understood implicitly that the effective quantum number of the open channel 3 has to be set equal to $i\infty$.

In Fig. 10 the time evolution of the autoionization rate $\gamma(t)$ is shown together with the corresponding zero- and one-photon contributions. The parameters chosen, i.e. $\varkappa^{-1} = 7$ ns $= 118 T_{\mathrm{orb}}$ and $\bar{\nu}_1 = 73$, $\mu_1 = 0.0$, $\mu_2 = 0.50 + i0.10$, correspond to typical values realizable
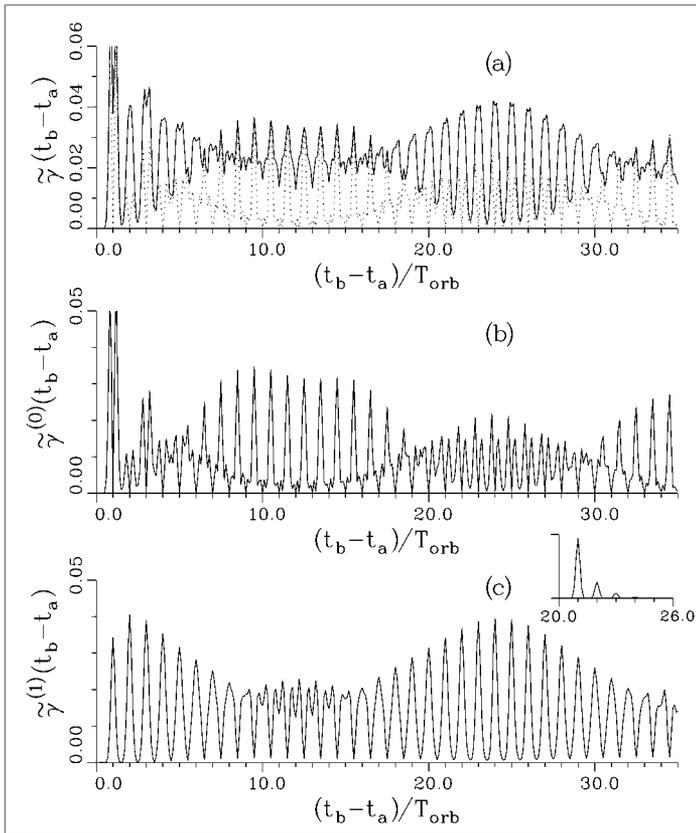
Figure 10: Autoionization under the condition of period matching of orbit time and Rabi period in the presence of spontaneous emission for parameters $T_{\text{Rabi}} = T_{\text{orb}}$, $\varkappa T_{\text{orb}} = 1/118$, $\bar{\nu}_1 = 73$ ($T_{\text{orb}} = 59$ ps), $\mu_1 = 0.0$, $\mu_2 = 0.50 + i0.10$, $\tau = 0.4T_{\text{orb}}$, $\varDelta = 0$. Fig. 10(a): total scaled autoionization rate $\tilde{\gamma} = \gamma T_{\text{orb}} \tau / |\mathscr{D}_{ge_1}^{(-)} \mathscr{E}^{(0)}|^2$ as obtained from the optical Bloch equations (full curve), total rate for $\varkappa = 0$ (dotted). Figs. 10(b) and (c): 0- and 1-photon contributions $\tilde{\gamma}^{(0)}$ and $\tilde{\gamma}^{(1)}$. Inset in Fig. 10(c): conditional autoionization rate $\gamma^{(1)}(t\,|\,t_1 = 20.5T_{\text{orb}})$.

in alkaline earth atoms [46]. The comparison of $\gamma(t)$ with the corresponding quantity in the absence of radiative damping (dotted curve of Fig. 10(a)) demonstrates that the influence of the spontaneous photon emission is significant already at interaction times of the order of T_{orb}. With the help of the zero- and one-photon contributions of Eqs. (48) this influence can be analyzed in detail. The zero-photon rate (Fig. 10(b)) vanishes at integer multiples of the mean classical orbit time T_{orb} because at these times the ionic core is in its ground state $|\Phi_1\rangle$. The maxima of Fig. 10(b) are due to fractions of the electronic Rydberg wave packet which are close to the atomic nucleus at times when the Rabi oscillating core is in its excited state $|\Phi_2\rangle$. These times are approximately given by $(m + \frac{1}{2})\,T_{\text{orb}}$, $m \in \mathbf{N}$. Revival effects are also visible. They take place at interaction times of the order of $25T_{\text{orb}}$. The one-photon rate of Fig. 10(c) exhibits maxima and minima at times mT_{orb} and $(m + \frac{1}{2})\,T_{\text{orb}}$. The maxima at integer multiples of T_{orb} reflect the fact that the photon is emitted spontaneously by the ionic core most probably when the electronic Rydberg wave packet is close to its outer turning point. Thus whenever the Rydberg electron returns to the atomic nucleus the ionic core is excited so that the Rydberg electron autoionizes with high probability (com-

pare inset in Fig. 10(c)). In the example considered in Fig. 10 the sum of zero- and one-photon contributions is indistinguishable from the corresponding numerical solution of the full optical Bloch equations.

3.3.   Electronic Rydberg wave packets and photon emission by the ionic core

In laser-induced two-electron excitation processes of the type shown in Fig. 8 radiative decay not only modifies the time evolution of an electronic Rydberg wave packet but vice versa the dynamics of the Rydberg electron can also affect the properties of the spontaneous photons emitted by the laser-excited core electron. This influence is expected to be particularly significant in cases where the electron correlation effects produced by the radiative core transitions, i.e. the shakeup, are large.

One way to describe the characteristics of the spontaneously emitted photons theoretically consists of applying the quantum-regression theorem [44] to the optical Bloch equations of Sec. 3.1. Thus, in principle all correlation functions of the spontaneously generated electromagnetic field can be evaluated. However, numerical problems may arise due to the presence of the ionization thresholds if Rydberg states are excited sufficiently close to threshold. Again, under such circumstances semiclassical path representations of the relevant N-photon transition amplitudes of the discussed in Sec. 3.1 might be a useful theoretical alternative. In the subsequent examples the influence of the dynamics of an electronic Rydberg wave packet on the radiative decay of the strongly bound core electron via electron correlation effects is discussed. All presented numerical examples have been obtained by applying the quantum-regression theorem and solving the relevant master equation in the energy representation. This is possible as in the subsequent examples the energies of the significantly excited Rydberg states are all located sufficiently well below threshold.

A characteristic quantity of the electromagnetic field generated by spontaneous emission of photons by the laser-excited ionic core is the intensity-intensity correlation function. This quantity is directly proportional to the atomic two-time correlation function $G^{(2)}(t_1, t_1 + \Delta t)$ $= \langle \sigma^{(+)}(t_1) \sigma^{(+)}(t_1 + \Delta t) \sigma^{(-)}(t_1 + \Delta t) \sigma^{(-)}(t_1) \rangle$ [44] ($\langle . \rangle$ indicates the statistical mean value and $\sigma^{(-)}(t)$ is the value of the transition operator $|\Phi_1\rangle \langle \Phi_2|$ at time t in the Heisenberg picture). This correlation function can be evaluated from the optical Bloch equations with the help of the quantum-regression theorem. In order to examine the influence of the dynamics of the Rydberg electron on the photon emission process by the core we consider a situation which has already been studied before in Sec. 3.2. We assume that a short laser pulse prepares an electronic Rydberg wave packet at time $t = 0$ in the presence of a cw-laser field which excites the ionic core resonantly. Afterwards the probability of observing two spontaneously emitted photons at times t_1 and $t_1 + \Delta t$ is investigated. However, we also assume that this two-time correlation function is measured provided that the Rydberg electron has not been ionized in the time interval of observation $(0, t_1 + \Delta t)$. If the ionized electron were not observed simultaneously with the spontaneously emitted photons, the two-time correlation function $G^{(2)}(t_1, t_1 + \Delta t)$ would not only contain information about electron correlation effects but also information about the trivial Rabi oscillations of the ionic core after the excited Rydberg electron has been ionized. The experimental realization of such a coincidence experiment involving ionized electron and spontaneously emitted photons may not be easy. Nevertheless for the sake of a complete theoretical understanding of the intricate interplay between electron correlation effects and spontaneous emission of photons in ICE processes this discussion is of interest.

In Fig. 11 the dependence of the correlation function $G^{(2)}(t_1, t_1 + \Delta t)$ on the time delay Δt is shown. The emission time of the first photon is chosen equal to the mean radiative damping time, i.e. $t_1 = \varkappa^{-1} = 5T_{\mathrm{orb}}$. Fig. 11(a) applies to equal quantum defects of the resonantly coupled core channels, i.e. $\mu_1 = \mathrm{Re}\,\mu_2$, whereas Fig. 11(b) corresponds to the
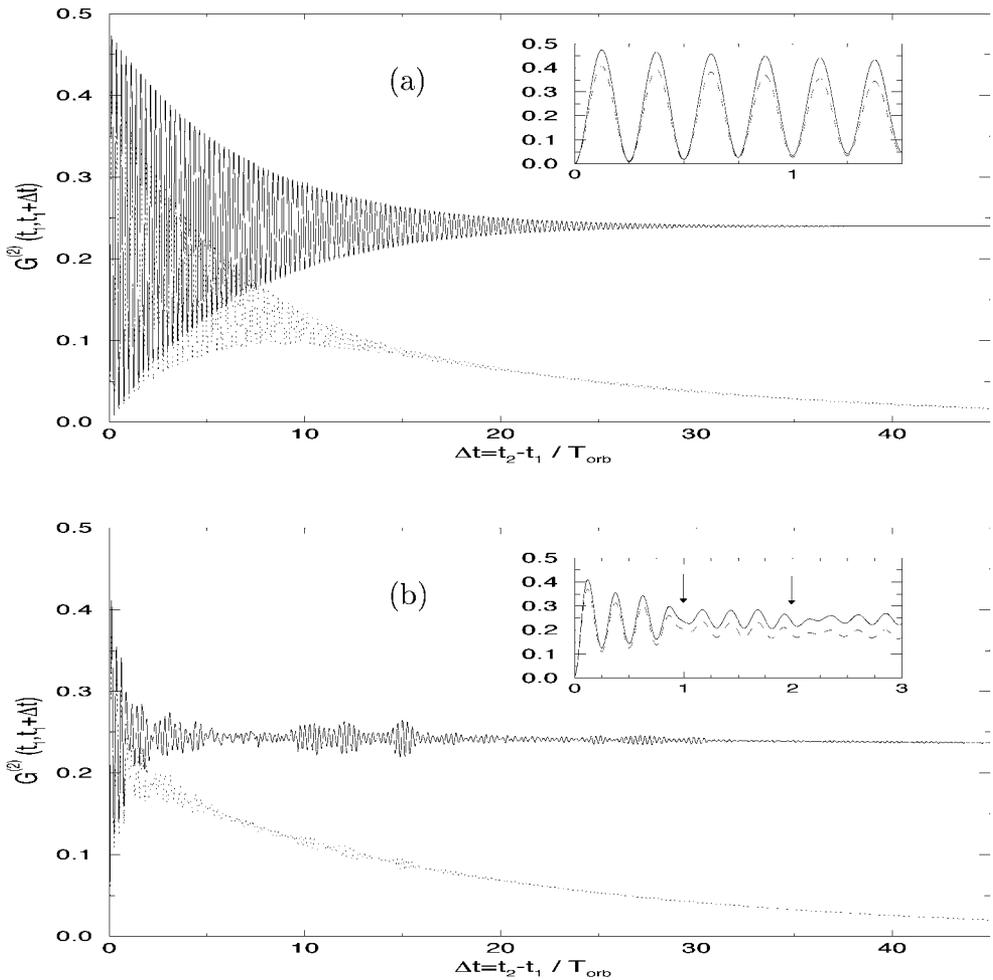
Figure 11: Second-order correlation function $G^{(2)}(t_1, t_1+\Delta t)$ for parameter values $t_1 = 5T_{\mathrm{orb}}$, $\bar{\nu}_1 = 171$, $\varkappa T_{\mathrm{orb}} = 1/5$, $T_{\mathrm{Rabi}} = 0.25 T_{\mathrm{orb}}$, $\Delta = 0$, $\mu_1 = 0.0$ and $\mathrm{Re}\,\mu_2 = 0.0$ (a), $\mathrm{Re}\,\mu_2 = 0.5$ (b). Full curves: $\mathrm{Im}\,\mu_2 = 0.0$, dotted curves: $\mathrm{Im}\,\mu_2 = 0.01$. The insets show the detailed behavior of the correlation function for small Δt. In the lower inset the wave packet recurrences are marked by arrows.

case of maximal shakeup, i.e. $\mu_1 = \mathrm{Re}\,\mu_2 + 0.5$. For the full curves autoionization is neglected, in the dotted curves it is taken into account with $\mathrm{Im}\,\mu_2 = 0.01$. In order to suppress effects of autoionization in these latter cases as much as possible the mean classical orbit time of the electronic Rydberg wave packet is synchronized with the Rabi period of the ionic core, i.e. $T_{\mathrm{orb}} = 4T_{\mathrm{Rabi}}$. It is apparent (and easily proved mathematically) that in the absence of electron correlation effects (Fig. 11(a)) the time dependence of the two-time correlation function $G^{(2)}(t_1, t_1 + \Delta t)$ exhibits the same behavior as in the case of a resonantly driven two-level system. Thus, the time evolution of the excited electronic Rydberg wave packet does not influence the characteristics of the photon emission by the second, strongly bound valence electron. The dotted curve indicates that autoionization leads to a global decrease of the observable signal. As soon as the quantum defects of both resonantly coupled core channels are no longer equal the excited electronic Rydberg wave packet

exerts a much stronger influence on the dynamics of the core valence electron. This influence of electron correlation effects on the process of photon emission is apparent from Fig. 11(b). Though in this case the positions of the maxima and minima of $G^{(2)}(t_1, t_1 + \Delta t)$ are still determined by the Rabi period of the ionic core the periodic motion of the electronic Rydberg wave packet leads to a modulation of these structures. These modulations are well recognizable in the inset of Fig. 11(b). There they are marked by arrows which appear at integer multiples of T_{orb}. Around $\Delta t = 14 T_{orb}$ and $\Delta t = 28 T_{orb}$ effects of fractional revivals of the electronic Rydberg wave packet are clearly visible ($\bar{\nu}_1 = 171 \rightarrow T_{rev}/T_{orb} = \frac{2}{3}\bar{\nu}_1 = 114$). Again autoionization of the excited Rydberg electron leads to an overall decrease of the detectable signal.

4.   Isolated Core Excitation and Atomic Center-of-mass Motion

4.1.   Introduction

The manipulation of the atomic center of mass motion with the help of light forces is one of the central topics of current research in quantum optics [32]. A main characteristic of the light forces is the fact that the momentum exchange between light field and atom proceeds essentially only by the excitation of the internal electronic degrees of freedom. This is due to the large mass difference between the atomic nucleus and the electrons. The resulting strong laser-induced correlation between the electronic dynamics of the atom and its center of mass motion offers the possibility of controlling the atomic motion in a wide variety of ways. Furthermore, it allows to examine the internal laser-modified electronic dynamics by observing the external degrees of freedom. In recent years major advances have been achieved especially with regard to the first of these aspects, e.g. in the techniques of cooling and trapping of atoms [47, 48] or in atomic beam manipulation with atom optical instruments [33].

So far, most investigations on the mechanical effects of light on atoms have been concerned with atomic few-level systems. However, it was shown recently in a number of articles [16, 49, 50] that systems with a high density of states such as Rydberg atoms may offer new and interesting perspectives in the context of atom optics. In these studies schemes for atomic beam deflection were investigated in which the coherent momentum transfer from a standing-wave laser field to the atom depends strongly on whether the laser field excites an isolated or a large number of Rydberg states. In the former case the momentum exchange is dominated by the wave aspects of the electronic dynamics, in the latter case by particle aspectgs of the Rydberg electron. So far investigations concentrated on laser excitation processes which involve a single valence electron only.

It is therefore natural to extend these studies to the case of laser-induced two-electron excitation processes and to examine their particular manifestations in the atomic center of mass motion. In view of the theoretical results summarized in Secs. 2 and 3 it suggests itself to turn to isolated core excitation processes first. In order to work out main aspects of the problem in a clear way we focus in the following on effects of the stimulated light force exerted on an atomic beam which traverses a standing light field. In the scheme under consideration the standing wave field drives the core transition, at the same time, however, the momentum transfer from the field to the atomic center of mass is modified by a previously excited Rydberg wave packet, which orbits around the core, and by the ensuing electron correlation effects, i.e. shakeup processes. To analyze these modifications in a convenient way a theoretical description of the atomic momentum distribution after leaving the standing wave is developed in Sec. 4.2. Thereby, the atomic motion is treated in the Raman-Nath approximation and the relevant transition amplitudes are expressed in terms of a semiclassical path expansion. In Sec. 4.3 this description is used to discuss basic physical effects electron correlations have on the center-of-mass motion. Aspects of possible experimental realizations are mentioned briefly.
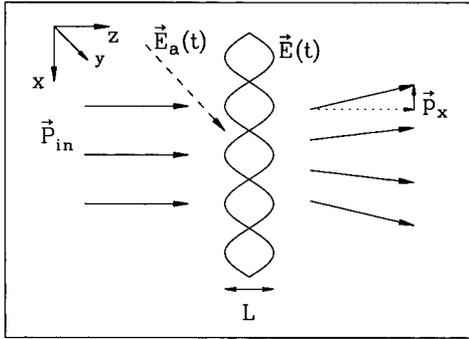
Figure 12: Setup for the model problem. After the atom has entered the standing wave field $\boldsymbol{E}(t)$, the short pulse $\boldsymbol{E}_a(t)$ is applied. By exciting the Rydberg wave packet the pulse triggers the Rabi oscillations of the core and thereby the momentum transfer to the atomic center of mass.

4.2.   Theoretical description of laser deflection by isolated core excitation

In order to present the main ideas most clearly in the following we discuss an idealized model problem which is depicted in Figs. 12 and 13. An alkaline earth atom with mass M and well defined initial momentum $\boldsymbol{P}_{\mathrm{in}}$ of its center of mass traverses a standing laser field at right angles. The standing wave will be approximated to be of rectangular shape with width L, i.e.

$$\boldsymbol{E}(\boldsymbol{R}, t) = \theta(z)\,\theta(L - z)\,\mathscr{E}(x)\,\boldsymbol{e}\,e^{-\omega t} + \text{c.c.} \tag{50}$$

with ω the light frequency, $\boldsymbol{e}$ the polarization and

$$\mathscr{E}(x) = \mathscr{E}_0 \sin{(kx)} \tag{51}$$

the field envelope. The atomic center of mass position will be denoted by $\boldsymbol{R} = (x, y, z)$. The modulus of the wave vector is given by k.

Initially, at $t = 0$ immediately before entering the standing wave, the atom is prepared in an energetically low lying bound electronic state $|g\rangle$ with energy ε_g. The standing wave field is assumed to be tuned in resonance with a transition of the ionic core from its ground state (energy ε_1) to an excited state (energy ε_2). Due to electron correlation effects, in
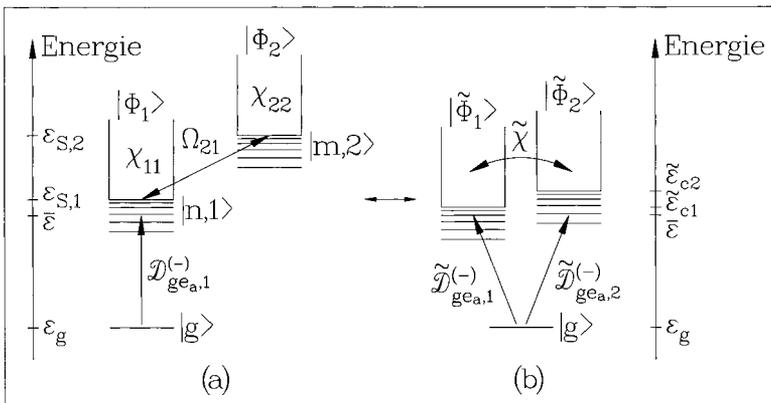

Figure 13: Excitation scheme for the internal atomic dynamics: (a) bare Rydberg series, (b) "dressed" Rydberg series.

general, the standing laser field will be well detuned from any excited state of the neutral atom. Thus, the light force exerted on the atom is negligible. After entering the standing wave the atom is exposed to a short (running wave) laser pulse

$$\boldsymbol{E}_a(t) = \mathscr{E}_a(t)\,\boldsymbol{e}_a\,e^{i(k_a y - \omega_a t)} + \text{c.c.} \tag{52}$$

with polarisation $\boldsymbol{e}_a$ and frequency ω_a which propagates with wave vector $k_a\boldsymbol{e}_y$ along the y-direction perpendicular to the incoming atom and the standing wave field. This choice of direction of propagation implies that the short pulse transfers at most one unit of photon momentum $k_a\boldsymbol{e}_y$ to the atom. The pulse envelope is centered around time t_0 and is taken to be of the form

$$\mathscr{E}_a(t) = \mathscr{E}_a^{(0)}\exp\left[-4(\ln 2)\,(t - t_0)^2/\tau^2\right] \tag{53}$$

with the pulse duration τ short in comparison with the time of flight of the atom through the standing laser field. The pulse is supposed to couple the ground state $|g\rangle$ to high lying Rydberg states close to the first photoionization threshold. If τ is small in comparison with the classical orbit time of these states, the short pulse creates an electronic Rydberg wave packet. In addition, however, the standing wave field will excite the ionic core resonantly as soon as the electronic wave packet is prepared. The subsequent Rabi oscillations of the ionic core will transfer momentum from the standing wave laser field to the atomic center of mass coherently by the stimulated light force. Contrary to the well known case of a resonantly coupled two-level system, this momentum transfer will be influenced by the dynamics of the electronic Rydberg wave packet via electron correlation effects, namely shakeup and autoionization. Thus when leaving the standing wave laser field the momentum distribution of the atom's center of mass will contain information about the dynamics of the Rydberg electron and the electron correlation effects during the interaction with the laser field.

The momentum distribution consists of three parts: if the atom was not excited by the short pulse, it leaves the standing wave essentially undeflected. If a Rydberg wave packet was created, the atom may leave the laser field with the core either in the ground or in the excited state. In the latter case the atom autoionizes quickly and the resulting ion is removed easily by an electric field. Therefore, a natural observable which contains information about the influence of the electron correlation effects on the center of mass motion is the momentum distribution of atoms which leave the standing wave with their core in the ground state. Further insights can be obtained if the measurement of the momentum distribution is performed state-selectivity with respect to the Rydberg electron, e.g. by means of ramped field ionization [18].

The interplay between laser-modified electron correlation effects and the atomic center of mass motion is exhibited in a particularly transparent way in the case of fast atoms. Atoms are considered to be fast if their kinetic energy is much larger than the electronic interaction energy with the exciting laser fields and if their deflection inside the laser field is small in comparison with the wave length of the standing wave. These conditions imply that inside the laser field the atomic center of mass moves with constant velocity $v_{\text{in}} = |\boldsymbol{P}|_{\text{in}}/M$ on a straight line trajectory perpendicular to the standing wave laser field. Under these conditions the Eikonal [51] and Raman-Nath [32] approximations can be used in the theoretical description. The state $\langle x\,|\,\psi(\mathscr{T})\rangle$ of an atom, which has crossed the standing wave laser field at position x with an effective interaction time of $\mathscr{T} = L/v_{\text{in}} - t_0$, may then be represented in the form

$$\langle x\,|\,\psi(\mathscr{T})\rangle = a_g^{(\mathscr{T})}(x)\,|g\rangle + \sum_n a_{n,1}^{(\mathscr{T})}(x)\,|n,1\rangle\,|\Phi_1\rangle + \sum_m a_{m,2}^{(\mathscr{T})}(x)\,|m,2\rangle\,|\Phi_2\rangle \tag{54}$$

(thereby, the two-channel excitation scheme of Fig. 13 has been used and the summations refer to both Rydberg and continuum states). In the spirit of the Eikonal and Raman-Nath approximation the probability amplitudes in the initial state $|g\rangle$, i.e. $a_g^{(\mathcal{T})}(x)$, and in the excited Rydberg states of channels 1 and 2, i.e. $a_{n,1}^{(\mathcal{T})}(x)$ and $a_{m,2}^{(\mathcal{T})}(x)$, are determined by solving the time dependent Schrödinger equation with Hamiltonian

$$H(x) = H_{\text{atom}} + V_{\text{ICE}}(x) + V_{\text{pump}}(t) \,. \tag{55}$$

In the two-channel approximation the atomic Hamiltonian is given by

$$H_{\text{atom}} = \varepsilon_g \, |g\rangle \, \langle g| + \sum_{j=1,2} (h_{jj} + V_{jj}(r) + \varepsilon_{cj}) \, |\Phi_j\rangle \, \langle \Phi_j| \tag{56}$$

(cf. Eqs. (13) and (14)). The coupling of channels 1 and 2 due to the laser-induced core excitation is described by the operator $V_{\text{ICE}}(x)$ defined according to Eq. (1) with the position-dependent, real-valued Rabi frequency

$$\Omega_{21}(x) = 2 \, \langle \Phi_2| \, \boldsymbol{d} \cdot \boldsymbol{e} \, |\Phi_1\rangle \, \mathscr{E}(x) \,. \tag{57}$$

The interaction of the atom with the short laser pulse which leads to the creation of the Rydberg wave packet is described by the operator

$$V_{\text{pump}}(t) = -\boldsymbol{d} \cdot \boldsymbol{e}_a \mathscr{E}_a(t) \, e^{-i\omega_a t} + \text{h.c.} \,. \tag{58}$$

For the sake of simplicity it is assumed that the pulse is sufficiently weak so that its effect on the atomic dynamics can be described in perturbation theory. In this case it is found [52]

$$a_{n,1}^{(\mathcal{T})}(x) = ie^{-i\bar{\varepsilon}t_0} \, \langle n, 1| \, \langle \Phi_1| \, e^{-iH_0(x)\mathcal{T}} \, \tilde{\mathscr{E}}_a(H_0(x) - \bar{\varepsilon}) \, \boldsymbol{d} \cdot \boldsymbol{e}_a \, |g\rangle \tag{59}$$

with the mean excited energy $\bar{\varepsilon} = \varepsilon_g + \omega_a$. The Fourier transform $\tilde{\mathscr{E}}_a(\varepsilon)$ of the short pulse envelope is defined in Eq. (11) and $H_0(x) = H_{\text{atom}} + V_{\text{ICE}}(x)$.

The probability amplitude of observing after its flight through the standing wave field a deflected atom in state $|n, 1\rangle \, |\Phi_1\rangle$ with transverse momentum p_x is given by [32]

$$a_{n,1}^{(\mathcal{T})}(p_x) = \frac{1}{\lambda} \int_0^\lambda dx \, a_{n,1}^{(\mathcal{T})}(x) \, e^{-ip_x x} \tag{60}$$

with $\lambda = 2\pi/k$ the wavelength of the standing wave. Eq. (60) shows how the state selective atomic transition amplitude $a_{n,1}^{(\mathcal{T})}(x)$ acts as a diffraction grating for the atomic center of mass motion. In order to exhibit clearly the influence of the electronic Rydberg wave packet on the atomic diffraction process it is convenient to express the transition amplitude in the form of a semiclassical path representation. It is given by [34]

$$a_{n,1}^{(\mathcal{T})}(x) = \frac{(-1)^{l+l}}{2\pi} \sum_{M=0}^{\infty} \int_{-\infty+i0}^{\infty+i0} d\varepsilon \, e^{-i\varepsilon\mathcal{T}} \, v_n^{-3/2} \times (e^{i\pi v_n} \boldsymbol{w}(x) - e^{-i\pi v_n} \boldsymbol{w}(x) \, e^{2\pi i \tilde{v}(x)})$$
$$\times (\tilde{\boldsymbol{\chi}}(x) \, e^{2\pi i \tilde{v}(x)})^M \, \tilde{\mathscr{D}}_{ge_a}^{(-)}(x) \, \tilde{\mathscr{E}}_a(\varepsilon_1 - \bar{\varepsilon}) \,. \tag{61}$$

In Eq. (61) l denotes the angular momentum of the Rydberg electron. The quantities $\tilde{\nu}(x)$, $\tilde{\chi}(x)$ and $\tilde{\mathcal{D}}_{ge_a}^{(-)}(x)$ characterize the excited Rydberg series in the presence of the continuous laser field $\boldsymbol{E}(\boldsymbol{R}, t)$ coupling the two channels. They refer to the description of the system in terms of the picture of dressed core states. Their definitions follow immediately from Eqs. (23), (30) and (31) of Sec. 2.2. Thereby, one has to take into account that the transformation matrix $\boldsymbol{O}$ between the dressed channels as well as the channel thresholds $\tilde{\varepsilon}_{cj}$ now depend on the position coordinate x due to the position-dependence of the Rabi frequency Ω_{21}. Explicitly, they are determined by the relation

$$\boldsymbol{O}^T(x) \begin{pmatrix} \varepsilon_{c1} & -\dfrac{1}{2}\,\Omega_{21}(x) \\ -\dfrac{1}{2}\,\Omega_{21}(x) & \varepsilon_{c2} \end{pmatrix} \boldsymbol{O}(x) = \tilde{\varepsilon}_c(x)\,. \tag{62}$$

The column vector $\boldsymbol{w}$ in Eq. (61) has components $w_i(x) = \boldsymbol{O}_{1i}(x)/(\varepsilon_{n,1} - \varepsilon_{c1} - \varepsilon + \tilde{\varepsilon}_{cj}(x))$. If the frequency ω of the standing wave fields is tuned in resonance with the core transition, $\tilde{\chi}(x)$ and $\tilde{\mathcal{D}}_{ge_a}^{(-)}(x)$ become independent of x. The effective quantum number of the Rydberg state $|n, 1\rangle\,|\Phi_1\rangle$ is denoted by $\nu_n = n - \mu_1$. Inserting Eq. (61) into Eq. (60) yields the semiclassical path representation for the transverse momentum distribution.

The physical interpretation of Eq. (61) follows directly from the discussion of Sec. 2.2. The M-th member of the sum in can be assigned to a process in which the Rydberg electron performs M complete orbital round trips around the nucleus after the initial excitation by the pump field. On each complete round trip in the dressed channel j the Rydberg electron acquires a phase of magnitude $2\pi\tilde{\nu}_{jj}(x)$ which is equal to the classical action of motion along a purely radial Kepler orbit with zero angular momentum and energy $\varepsilon - \tilde{\varepsilon}_{cj}(x) < 0$. Between two round trips the Rydberg electron may be scattered by the Rabi-oscillating ionic core. This process is described by the scattering matrix $\tilde{\chi}(x)$. During the $(M+1)$-th round trip the atom leaves the standing wave field and the state of the Rydberg electron is projected onto the bare Rydberg states $|n, 1\rangle\,|\Phi_1\rangle$. This projection is described by the first bracketed term in the second line of Eq. (61). Finally, the spatial dependence of the probability amplitudes $a_{n,1}^{(\mathcal{F})}(x)$ determines the momentum distribution of the deflected atoms according to Eq. (60). One should note the formal similarity between Eq. (61) and the expressions (45) and (46) (after performing the integration over τ in Eq. (46)) for the time-independent transition amplitude $T_{fg}^{(1)}$ pertaining to a pump-probe process with an intermediate spontaneous photon emission. This similarity is due to the fact that the atom's leaving the standing wave as well as the spontaneous photon emission are described as events of negligible duration which may occur at every instant during the round trip of the wave packet around the core.

4.3.   Electron correlation effects and atomic momentum distributions

In this subsection we examine the physical implications of the theoretical description which was given for atomic laser deflection by laser-induced core transitions in Sec. 4.2. For the sake of clarity the discussion is again restricted to the two-channel excitation scheme depicted in Fig. 13. This is justified as long as one is interested in interaction times between atom and standing wave which are of the order of several wave packet orbit times. In this case effects of autoionization are expected to be small [29] (see also Sec. 2.3). However, these effects as well as direct photoionization of the Rdberg electron could easily be incorporated into the formalism with the help of complex and intensity-dependent quantum defects [15]. In view of typical values for spontaneous lifetimes the influence of spontaneous

emission processes (which would be more difficult to take into account) may also be neglected.

More attention must be paid to the question of how to realize the scheme for beam deflection shown in Fig. 12 experimentally. If one used a cw-laser to create the standing wave, then the laser beam would have to be focused onto a diameter of the order of 10^{-7} m to achieve an interaction time of 100 ps ($\simeq T_{orb}$) for a beam velocity of 1000 m/s. In Ref. [35] it was argued that this and other difficulties could be circumvented by realizing the standing wave with the help of two counter-propagating short laser pulses. As soon as these pulses overlap and create the standing wave the short pump pulse is applied. This experimental setup which should produce essentially the same momentum distributions as the theoretical model of Sec. 4.2 would offer several advantages: first of all, it would not be necessary that only a single atom interacts with the pump pulse and the standing wave a time. Instead, one can use an atomic beam of higher intensity as the atom-laser interaction time is only determined by the timing and the temporal profile of the three short pulses and not by the atomic position and velocity. For the same reason the experiment should also be rather insensitive to the longitudinal velocity spread of the beam. Furthermore the use of short pulses allows to achieve high field intensities easily and it would not be necessary to focus the pulses tightly. In view of the rapid progress in the field of manufacturing and manipulating short pulses [53] an actual realization of this setup appears to be within reach in the near future.

In the following numerical examples the influence is examined which the laser-induced electron correlations exert on the momentum transfer between laser field and atom for various degrees of shakeup. Thereby, resonant core excitation ($\Delta = \varepsilon_{c2} - \varepsilon_{c1} = 0$) and a Rydberg wave packet with mean quantum number $\bar{\nu}_1 = [2(\varepsilon_{c1} - \bar{\varepsilon})]^{-1/2} = 80$ and $\mu_1 = 0.0$ are considered. The duration τ of the short pulse is equal to $0.3 T_{orb}$ with $T_{orb} = 2\pi\bar{\nu}_1^3 = 77.8$ ps unless otherwise stated. The form (51) of the envelope of the standing wave field implies that the distribution of transverse momenta p_x of an atom leaving the interaction region with is core in the ground state contains only components equal to even multiples of the photon momentum k. This momentum distribution is symmetric with respect to $p_x = 0$. In the following examples only the part of the momentum distribution with $p_x \geq 0$ is shown. For the sake of clarity it is depicted in the form of a continuous curve instead of discrete points at even multiples of k.

Minimum shakeup correlations, i.e. $\mu_2 - \mu_1 = 0.0$: In this case the dressed scattering matrix is a multiple of the unit matrix, i.e. $\hat{\chi}(x) = e^{2i\pi\mu_1}\mathbf{1}$. Even though no core scattering takes place between the dressed Rydberg series the momentum transfer to the atomic center of mass is determined by the characteristics of the electronic wave packet prepared. To discuss this momentum transfer it is convenient to sum up the geometric series in Eq. (61) which yields for the position-dependent probability amplitude

$$a_{n,1}^{(\mathcal{T})}(x) = (-1)^l \frac{d_{\varepsilon g}}{2\nu_n^{3/2}} \left[e^{-i\bar{\varepsilon}_{n,+}(x)\mathcal{T}} \, \tilde{\mathcal{E}}_a(\tilde{\varepsilon}_{n,+}(x) - \bar{\varepsilon}) + e^{-i\bar{\varepsilon}_{n,-}(x)\mathcal{T}} \, \tilde{\mathcal{E}}_a(\tilde{\varepsilon}_{n,-}(x) - \bar{\varepsilon}) \right]. \qquad (63)$$

This way the probability amplitude is expressed in terms of the contributions of the two dressed states $|n, \pm\rangle = \frac{1}{\sqrt{2}}(|n, 1\rangle \mp |n, 2\rangle)$ in the standing wave field pertaining to the two bare states $|n, 1(2)\rangle$. Their energies are given by $\tilde{\varepsilon}_{n,\pm}(x) = \varepsilon_{c1} \pm \frac{1}{2}\Omega_{21}(x)$. The dipole matrix element between the initial state $|g\rangle$ and an energy-normalized continuum state $|\varepsilon\rangle$ in the bare channel 1 is denoted by $d_{\varepsilon g}$. According to Eq. (63) one can distinguish three limiting cases:

(a) $1/\tau \gg \Omega_{21,\max}$: The energy spread $1/\tau$ of the prepared wave packet is much larger than the maximum Rabi frequency $\Omega_{21,\max}$. In this case one may approximate $\tilde{\mathcal{E}}_a(\tilde{\varepsilon}_{n,+}(x) - \bar{\varepsilon}) \approx \tilde{\mathcal{E}}_a(\tilde{\varepsilon}_{n,-}(x) - \bar{\varepsilon}) \approx \tilde{\mathcal{E}}_a(\varepsilon_{n,1} - \bar{\varepsilon})$ (cf. Fig. 14(a)). Therefore the deflection pattern is almost indistinguishable from the well-known one of a fast two-level atom which
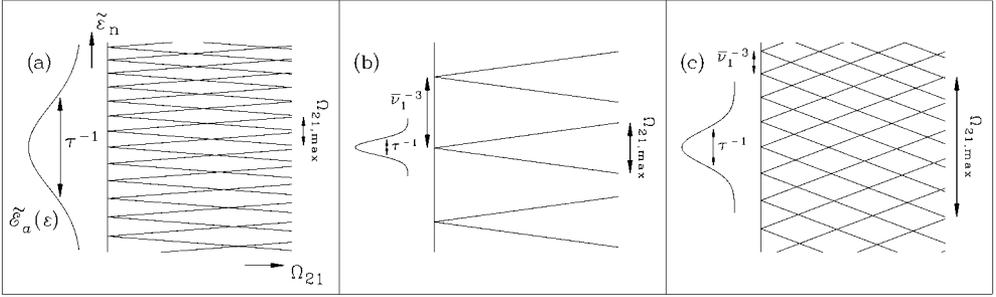
Figure 14: The relation between the maximum induced Rabi frequency $\Omega_{21,\text{max}}$, the excited energy range τ^{-1} and the distance between adjacent bare Rydberg states $\bar{\nu}_1^{-3} = 2\pi/T_{\text{orb}}$ determines the characteristics of the momentum distribution in the case of equal quantum defects. This interplay is indicated by displaying the laser pulse shape $\tilde{\mathscr{E}}_a$ and the relevant excited dressed states energies $\tilde{\varepsilon}_n$ as a function of Ω_{21} for the cases (a), (b) and (c) discussed in the text.

enters a standing wave field (of rectangular shape) in its ground state and interacts with it for a time $\mathscr{T}$ [32]. As an example, in Fig. 15(a) the state-selective momentum distribution $P_{n,1}^{(\mathscr{T})}(p_x) = |a_{n,1}^{(\mathscr{T})}(p_x)|^2$ and the total distribution $P_1^{(\mathscr{T})}(p_x) = \sum_{n_1} P_{n,1}^{(\mathscr{T})}(p_x)$ summed over all Rydberg states are shown for $T_{\text{Rabi}} = 0.1T_{\text{orb}} > \tau = 0.03T_{\text{orb}}$. They display the rapid oscillations familiar from the above-mentioned two-level case. The distributions $P_{n,1}^{(\mathscr{T})}(p_x)$ differ from each other only by a multiplicative constant which is due to the energy dependence of the envelope function $\tilde{\mathscr{E}}_a(\varepsilon)$.

(b) $1/\tau \gg \Omega_{21,\text{max}} < 2\pi/T_{\text{orb}}$: This condition implies that in general only at most one pair of dressed states belonging to a certain principal quantum number n is excited (Fig. 14(b)). The momentum distribution could also be obtained from a pure two-level system which is excited correspondingly from a low-lying state. However, due to the strong position dependence of the excitation amplitudes $\tilde{\mathscr{E}}_a(\tilde{\varepsilon}_{n,\pm}(x) - \bar{\varepsilon})$ interesting effects may be observed. If one chooses, for example, $\bar{\varepsilon}$ equal to the energy of a bare Rydberg state, i.e. $\bar{\varepsilon} = \varepsilon_{n,1}$, then the atom is excited to the two dressed Rydberg states $|n, \pm\rangle$ only in the
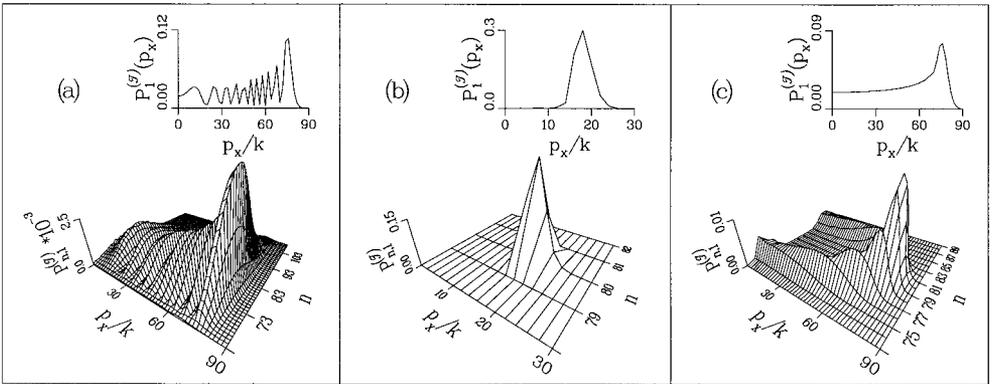

Figure 15: State-selective momentum distributions $P_{n,1}^{(\mathscr{T})} = |a_{n,1}^{(\mathscr{T})}|^2$ and total momentum distributions $P_1^{(\mathscr{T})} = \sum_n P_{n,1}^{(\mathscr{T})}$ (both in units of $|(\mathscr{D}_{ge_a}^{(-)})_1 \mathscr{E}_a^{(0)}|^2 \tau$) for $\mu_1 = \mu_2 = 0.0$, $\bar{\nu} = 80$, $\Delta = 0$ and (a) $\mathscr{T} = 2.5T_{\text{orb}}$, $T_{\text{Rabi,min}} = 0.1T_{\text{orb}}$, $\tau = 0.03T_{\text{orb}}$; (b) $\mathscr{T} = 6.0T_{\text{orb}}$, $T_{\text{Rabi,min}} = 1.0T_{\text{orb}}$, $\tau = 2.0T_{\text{orb}}$; (c) $\mathscr{T} = 2.5T_{\text{orb}}$, $T_{\text{Rabi,min}} = 0.1T_{\text{orb}}$, $T = 0.3T_{\text{orb}}$.

vicinity of the field nodes. There the induced light force (and thus the deflection) is large while the excitation in regions of weak induced light force is suppressed. In this way an efficient beam splitter is realized (Fig. 15(b)). The maximum momentum transferred is approximately given by $|p_x|_{\text{max}} = k\Omega_{21,\text{max}}\mathcal{T}/2$.

(c) $1/\tau \ll \Omega_{21,\text{max}}$ and $\Omega_{21,\text{max}} > 2\pi/T_{\text{orb}}$: Due to the second condition a number of dressed states with different principal quantum numbers n are excited significantly and, as expressed by the first condition, their excitation amplitudes vary strongly with position (Fig. 14(c)). The resulting momentum distribution cannot be obtained with a two-level system and thus reflects the presence of the Rydberg wave packet. Fig. 15(c) shows that the atomic deflection is indeed selective with respect to the Rydberg states. Dressed states of principal quantum number n with $|\varepsilon_{n,1} - \bar{\varepsilon}| < 1/\tau$ are excited only in the vicinity of the field nodes and are deflected strongly as described in case (b). States with $\Omega_{21,\text{max}} > |\varepsilon_{n,1} - \bar{\varepsilon}| > 1/\tau$ are excited only in regions of weak stimulated light force and are therefore less deflected.

Maximum shakeup correlations, i.e. $\mu_2 - \mu_1 = 0.5$: In this case the corresponding dressed scattering matrix is given by

$$\tilde{\chi}(x) = e^{2i\pi(\mu_1 + \mu_2)} \begin{pmatrix} 0 & 1 \\ 1 & 0 \end{pmatrix}. \tag{64}$$

It is independent of the position x at which the atom crosses the standing wave field because of the resonant character of the excitation. With each return to the core region the fractions of the initially prepared electronic Rydberg wave packet which propagate in the photon dressed core channels are scattered from one channel into the other one with a probability of unity. This extreme case of core scattering influences the momentum distribution of a diffracted atom significantly. In this context it is particularly interesting to study the width of the momentum distribution as a function of the interaction time between standing wave field and atom. This question is conveniently examined with the help of the semiclassical path expansion for the transverse momentum distribution given by Eqs. (60) and (61). The results of the analysis which is detailed in Ref. [35] and which is based on a stationary phase evaluation of the semiclassical path expansion may be summarized as follows:

(1) at interaction times equal to a small odd multiple of T_{orb}, i.e. $\mathcal{T} = (2N + 1) T_{\text{orb}}$ with integer values of N up to about 5, to a good degree of approximation the maximum transferred momentum $|p_x|_{\text{max}}$ is given by

$$|p_x|_{\text{max}} = \frac{1}{2} k\Omega_{21,\text{max}} T_{\text{orb}}. \tag{65}$$

This value is independent of N. Like in the case of vanishing shakeup the maximum momentum originates from atoms which cross the standing wave at the field nodes.

(2) at interaction times equal to a small even multiple of T_{orb} the relation

$$|p_x|_{\text{max}} = \frac{3}{8} k\Omega_{21,\text{max}}^2 \mathcal{T} \left(\frac{T_{\text{orb}}}{2\pi}\right)^{2/3} \tag{66}$$

holds. This result also applies to the case of large interaction times, irrespective of whether the number of returns is even or odd. The maximum transverse momentum of Eq. (66) grows linearly with $\mathcal{T}$. It is associated with atoms which cross the standing wave at positions with $\sin(2kx) = 0$ at which the electric field strength does not vanish.

For interaction times $\mathcal{T}$ up to the order of several T_{orb} and maximum Rabi frequencies comparable to the mean excited level spacing $\bar{\nu}_1^{-3}$ Eqs. (65) and (66) imply that the max-
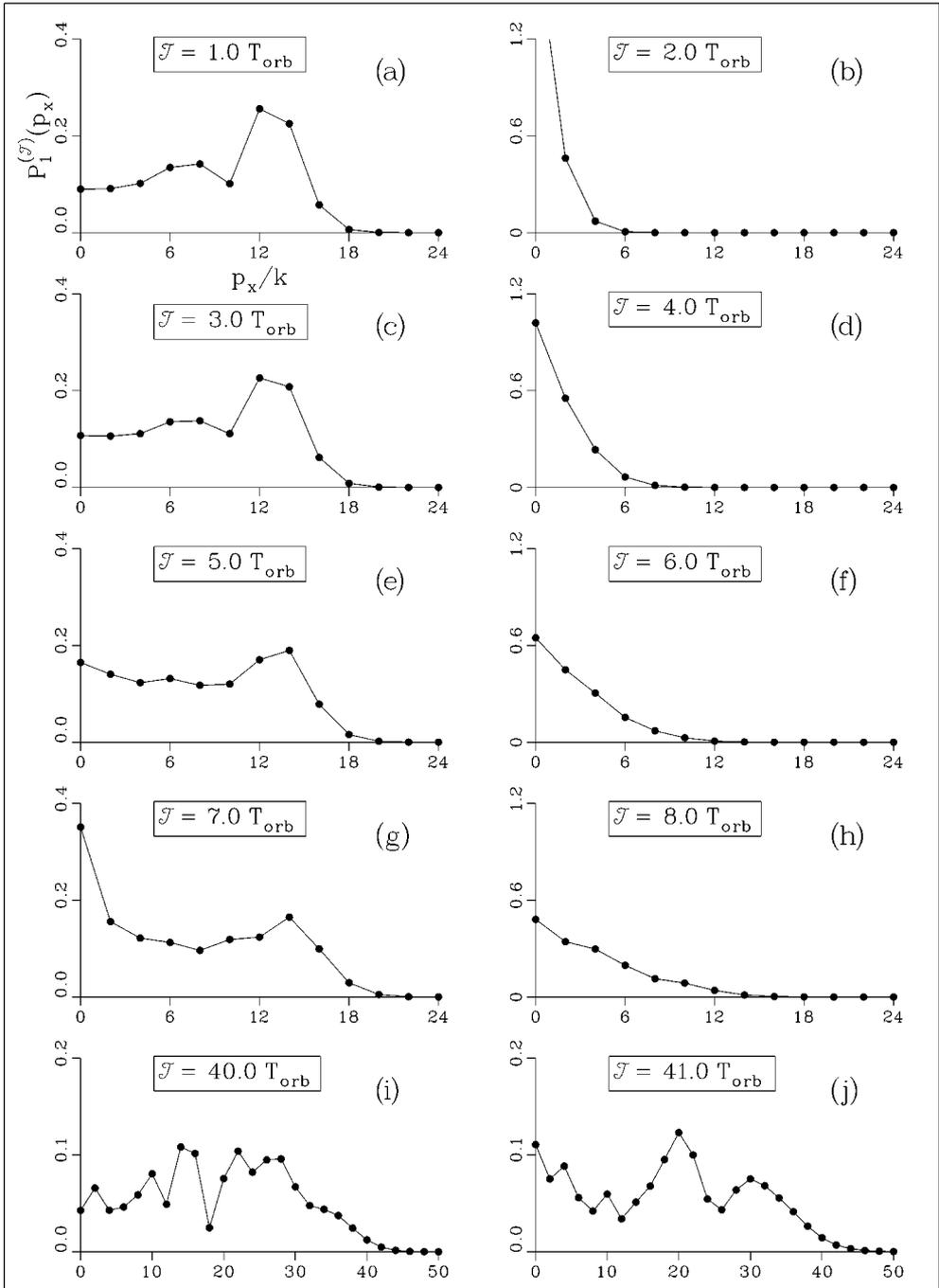
Figure 16: Total momentum distribution $P_1^{(\mathscr{T})}(p_x)$ for parameters $\mu_1 = 0.0$, $\mu_2 = 0.5$, $T_{\text{Rabi, min}} = 0.2T_{\text{orb}}$ and various interaction times $\mathscr{T}$ (other parameter values as given in the text).

imum momentum transferred at odd multiples of T_{orb} is significantly larger than the one transferred at even multiples. The transverse momentum distribution is thus of oscillating width with respect to the interaction time. The laser-induced scattering process between the electronic Rydberg wave packet and the excited core electron causes the time evolution of the momentum transfer from the standing wave laser field to the atom to be reversed at each return of the wave packet to the core. For larger interaction times the oscillations in the width of the distribution are gradually washed out. The core scatterings then manifest themselves in the fact that the maximum momentum transferred is much smaller than it would be in the absence of shakeup.

These characteristic features are exemplified in Fig. 16 where total momentum distributions $P_1^{(\mathcal{T})}(p_x)$ are depicted for $T_{Rabi, min} = 0.2T_{orb}$ and different values of interaction times with the standing laser field. Figs. 16(a, c, e, g) on the one hand and Figs. 16(b, d, f, h) on the other hand illustrate the oscillation of the width of the momentum distribution as a function of the interaction time. They also confirm the more detailed predictions of Eqs. (65) and (66) as they show $|p_x|_{max}$ to be approximately constant for odd multiples of T_{orb} while it increases proportional to $\mathcal{T}$ at even multiples. The corresponding proportionality constant and the width of the distribution at odd multiples of T_{orb} are also in good quantitative agreement with the values inferred from Eqs. (65) and (66). Figs. 16(i) and (j) confirm the validity of Eq. (66) at large interaction times.

Intermediate shakeup correlations, i.e. $0.0 < \mu_2 - \mu_1 < 0.5$: For an intermediate difference in quantum defects the dressed scattering matrix can be decomposed into a diagonal and an off-diagonal part, i.e. $\tilde{\chi} = \tilde{\chi}_{diag} + \tilde{\chi}_{off}$. This decomposition reflects the fact that at each return to the nucleus the Rydberg wave packet may either be scattered between the dressed channels ($\tilde{\chi}_{off}$) or not ($\tilde{\chi}_{diag}$). As the foregoing discussion has shown both processes have completely different effects on the momentum transfer from the standing wave field to the atomic center of mass. As long as the core has not experienced a scattering of the wave packet between the dressed channels the momentum distribution grows linearly with time. However, as soon as such a scattering has taken place the momentum transfer is "reversed" and the momentum distribution begins to shrink. Subsequent scattering events lead to further characteristic modifications in the momentum transfer. As the events of scattering and non-scattering are superposed quantum mechanically, the momentum distribution consists of a superposition of the various distinct deflection patterns arising from the different "scattering histories". Therefore, the internal dynamics of the atom which is determined by the interaction between the Rydberg wave packet and the ionic core is reflected in detail in the momentum distribution of the atomic center of mass motion.

The quantitive analysis of these kinds of processes may be accomplished easily with the help of Eqs. (60) and (61). As an example Fig. 17(a) shows the momentum distribution for an atom with $\mu_2 - \mu_1 = 0.20$ and interaction time $\mathcal{T} = 1.7T_{orb}$. In this case only the $M = 1$-term in Eq. (61) contributes significantly to the probability amplitude. The momentum distribution consists essentially of two distinct peaks around $p_x \approx 0$ and $p_x \approx 50k$. Using the decomposition of the dressed scattering matrix the inner peak can be attributed to atoms in which the wave packet fractions have experienced a scattering between the dressed channels at their first return to the nucleus. The outer peak corresponds to atoms with unscattered wave packet fractions (Fig. 17(b)). Thus, the internal dynamics is mapped onto the momentum distribution in a clear way. Figs. 17(c), (d) show the analysis of a more complicated deflection pattern at time $\mathcal{T} = 2.5T_{orb}$, where $M = 2$ is dominant, in terms of the different histories connected with two wave packet returns to the core. In this example, a time of approximately $0.5T_{orb}$ has elapsed since the second return. The width of the contribution pertaining to atoms which have experienced no scatterings of the wave packet fractions between the dressed channels ($\times$) continues to grow linearly with $\mathcal{T}$. The distribution corresponding to a scattering at the second return ($\triangle$), on the other hand, has begun to shrink due to the "reversal" effect. The distributions for scattering at the first return ($\circ$, $\diamond$)
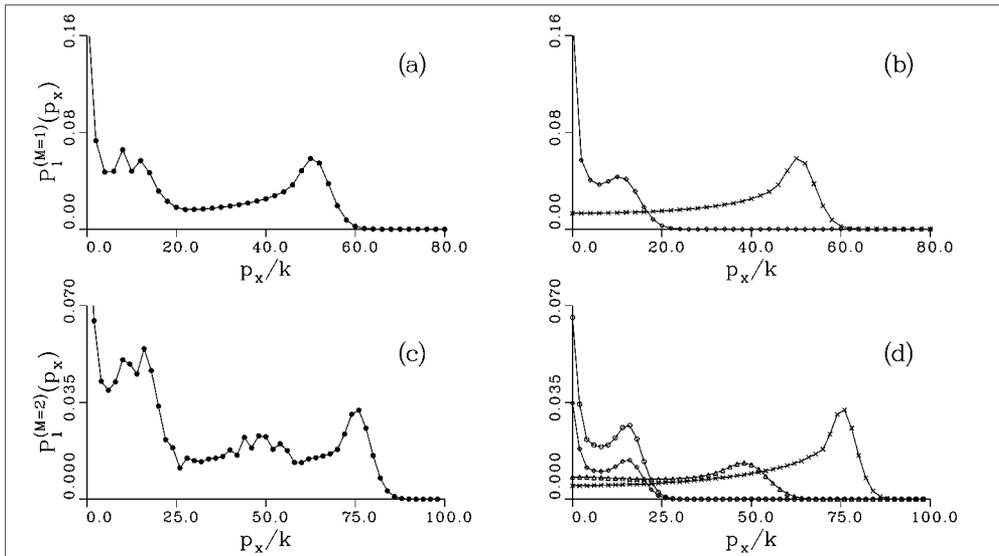
Figure 17: (a): $M = 1$-contribution $P_1^{(M=1)}$ (as evaluated from Eqs. (60) and (61)) to the total momentum distribution $P_1^{(\mathcal{T})}$ for parameters $\mu_1 = 0.0$, $\mu_2 = 0.2$, $T_{\text{Rabi}} = 0.1T_{\text{orb}}$ and interaction time $\mathcal{T} = 1.7T_{\text{orb}}$ (other parameters as given in the text). (b): Contributions to $P_1^{(M=1)}$ from atoms in which the Rydberg wave packet has been scattered between the dressed channels at the first return to the core ($\diamondsuit$, evaluated by replacing $\tilde{\chi}$ by $\tilde{\chi}_{\text{off}}$ in Eq. (61)) and atoms in which the wave packet leave the core unscattered ($\times$, evaluated with $\tilde{\chi}_{\text{diag}}$). (c): same as (a) for $M = 2$ and $\mathcal{T} = 2.5T_{\text{orb}}$. (d): Contributions to $P_1^{(M=2)}$ from atoms in which the wave packet has been scattered between the dressed channels twice ($\diamondsuit$), only at the first return ($\bigcirc$), only at the second return ($\triangle$), neither at the first nor the second return ($\times$).

are both rather narrow because the corresponding atoms did not possess any transverse momentum at the time of the second return of the wave packet. However, their width increases with growing interaction time.

In Ref. [35] it is shown that the notion of the "reversal effect" may be cast into a more precise form. To this end, one considers the maximum transverse momentum $|p_x|_{\text{max}}$ of a contribution to the momentum distribution which is characterized by a given sequence of scattering and non-scattering events in the course of the wave packet's returns to the core. A set of rules can then be constructed with the help of which $|p_x|_{\text{max}}$ may be determined. These rules allow one to analyze complex structures in the momentum distribution quantitatively in a simple way. Furthermore, they confirm the idea which was put forward above that after a core scattering the momentum distribution will shrink (grow) as a function of the interaction time $\mathcal{T}$ if it has been growing (shrinking) before. If the wave packet does not experiene a core scattering at its return to the nucleus the momentum distribution continues to grow or to shrink, respectively.

5.   Summary and Outlook

Isolated core excitation processes offer interesting possibilities for investigating electron correlation effects and their modification by intense laser fields. In this article recent theoretical work on this problem has been reviewed. The presentation focused on time-dependent

manifestations of such ICE-modified correlation effects in connection with the dynamics of an electronic Rydberg wave packet. It was shown that for this purpose the nonperturbative ICE processes and the electron dynamics can be described in a physically transparent way by a combination of quantum defect theory, semiclassical and stochastic methods. Thus a unified theoretical understanding of various aspects of laser-modified electron correlation effects in ICE processes is obtained. In this review three aspects have been discussed in detail, namely ICE processes in intense laser fields, ICE processes and radiative damping of the ionic core and ICE processes and the influence of the resulting stimulated light force on the atomic center of mass motion. The common framework for these topics was provided by an excitation scheme in whih after preparing the Rydberg wave packet the ionic core is resonantly driven by an intense laser field. It was shown that via the electron correlation effects the Rydberg electron may be used as a sensitive probe for the time evolution of the ionic core. Vice versa, the external laser manipulation of the core allows for a coherent control of the Rydberg wave packet. Laser-induced suppression of autoionization provides an important example in this respect. In addition, this effect is very well suited for the study of processes which destroy the coherence of the atomic system, in particular sponta-neous photon emission of the core. The entanglement wave packet and core dynamics is also reflected in the atomic center of mass motion. In conclusion, the examples presented demonstrate the richness of quantum-optical phenomena which may be exhibited by core-excited Rydberg system.

There are various directions into which the work presented in this article may be ex-tended. For example, wave packet dynamics under the combined influence of isolated core excitation and external static fields should lead to new and interesting effects. This way it would be possible to manipulate the electron dynamics both inside and outside the core region at the same time. Furthermore, one can consider more complicated excitation pro-cesses of the inner electron by which it is excited into coherent superpositions of several core states. Ultimately, this would lead to studies on the correlated dynamics of two electro-nic wave packets. The pursuit of this direction will allow one to study the transition from dynamical cases in which the problem can be described within the framework of ICE models to cases in which the system constitutes a complicated three-body Coulomb pro-blem. As to atom optical applications it suggests itself to consider the perspectives of ICE processes for the study of cold atoms. In this context they could possibly be used for the trapping of Rydberg atoms, for example.

Acknowledgments

References

[1] G. ALBER and P. ZOLLER, Phys. Rep. **199**, 231 (1991).
[2] M. J. SEATON, Rep. Prog. Phys. **46**, 167 (1983).
[3] U. FANO and A. R. P. RAU, *Atomic Collisions and Spectra* (Academic Press, New York, 1986).
[4] J. DUBAU and M. J. SEATON, J. Phys. B **17**, 381 (1984).
[5] A. TEN WOLDE, L. D. NOORDAM, A. LAGENDIJK, and H. B. VAN LINDEN VAN DEN HEUVELL, Phys. Rev. Lett. **61**, 2099 (1988).
[6] J. A. YEAZELL and C. R. STROUD, Phys. Rev. Lett. **60**, 1494 (1988).
[7] J. A. YEAZELL, M. MALLALIEU, and C. R. STROUD, Phys. Rev. Lett. **64**, 2007 (1990).
[8] L. MARMET, H. HELD, G. RAITHEL, J. A. YEAZELL, and H. WALTHER, Phys. Rev. Lett. **72**, 3779 (1994).

[9] H. H. Fielding, J. Wals, W. J. van der Zande, and H. B. van Linden van den Heuvell, Phys. Rev. A **51**, 611 (1995).
[10] G. Alber, Z. Phys. D **14**, 307 (1989).
[11] G. Alber, Phys. Rev. A **40**, 1321 (1989).
[12] W. E. Cooke, T. F. Gallagher, S. A. Edelstein, and R. M. Hill, Phys. Rev. Lett. **40**, 178 (1978).
[13] W. A. Henle, H. Ritsch, and P. Zoller, Phys. Rev. A **36**, 683 (1987).
[14] D. W. Schumacher, R. I. Duncan, R. R. Jones, and T. F. Gallagher, J. Phys. B **29**, L397 (1996).
[15] G. Alber and P. Zoller, Phys. Rev. A **37**, 377 (1988).
[16] G. Alber, W. T. Strunz, and O. Zobay, Mod. Phys. Lett. B **8**, 1461 (1994).
[17] G. Alber and B. Eggers, to appear in Phys. Rev. A.
[18] T. F. Gallagher, *Rydberg Atoms* (Cambridge University Press, 1994).
[19] F. Robicheaux, Phys. Rev. A **47**, 1391 (1993).
[20] N. J. van Druten and H. G. Muller, Phys. Rev. A **52**, 3047 (1995).
[21] N. J. van Druten and H. G. Muller, J. Phys. B **29**, 15 (1996).
[22] X. Wang and W. E. Cooke, Phys. Rev. Lett. **67**, 976 (1991); X. Wang and W. E. Cooke, Phys. Rev. A **46**, R2201 (1992); X. Wang and W. E. Cooke, Phys. Rev. A **46**, 4347 (1992).
[23] J. G. Story, D. I. Duncan, and T. F. Gallagher, Phys. Rev. Lett. **71**, 3431 (1993).
[24] See, e.g., S. L. Haan, M. Bolt, H. Nymeyer, and R. Grobe, Phys. Rev. A **51**, 4640 (1995); B. Walker, M. Kaluza, B. Sheehy, P. Agostini, L. F. DiMauro, Phys. Rev. Lett. **75**, 633 (1995); L. G. Hanson, J. Zhang, and P. Lambropoulos, Phys. Rev. A **55**, 2232 (1997).
[25] R. R. Jones and P. H. Bucksbaum, Phys. Rev. Lett. **67**, 3215 (1991).
[26] H. Stapelfeldt, D. G. Papaioannou, L. D. Noordam, and T. F. Gallagher, Phys. Rev. Lett. **67**, 3223 (1991).
[27] S. A. Bhatti, C. L. Cromer, and W. E. Cooke, Phys. Rev. A **24**, 161 (1981).
[28] R. H. Bell and M. J. Seaton, J. Phys. B **18**, 1589 (1985).
[29] O. Zobay and G. Alber, Phys. Rev. A **52**, 541 (1995).
[30] L. G. Hanson and P. Lambropoulos, Phys. Rev. Lett. **74**, 5009 (1995).
[31] O. Zobay and G. Alber, Phys. Rev. A **54**, 5361 (1996).
[32] A. P. Kazantsev, G. I. Surdutovich, and V. P. Yakovlev, *Mechanical Action of Light on Atoms* (World Scientific, Singapore, 1990).
[33] C. Adams, M. Sigel and J. Mlynek, Phys. Rep. **240**, 143 (1994).
[34] O. Zobay, Ph.D. dissertation, Universität Freiburg im Breisgau (1996).
[35] O. Zobay and G. Alber, submitted to Phys. Rev. A.
[36] L. D. Noordam, D. I. Duncan, and T. F. Gallagher, Phys. Rev. A **45**, 4734 (1992).
[37] A. Dalgarno and J. T. Lewis, Proc. R. Soc. London, Ser. A **233**, 70 (1955).
[38] L. G. Hanson, J. Zhang, and P. Lambropoulos, Phys. Rev. A **55**, 2232 (1997).
[39] A. Giusti-Suzor and P. Zoller, Phys. Rev. A **36**, 5178 (1987).
[40] N. H. Tran, P. Pillet, R. Kachru, and T. F. Gallagher, Phys. Rev. A **29**, 2640 (1984).
[41] W. Sandner, Comments At. Mol. Phys. **20**, 171 (1987).
[42] T. Baumert, M. Strehle, U. Weichmann, and G. Gerber, Verhandl. DPG (VI) **32**, 197 (1997).
[43] R. Scheunemann, Diploma thesis, Universität Freiburg im Breisgau (1996).
[44] B. R. Mollow, Phys. Rev. A **12**, 1919 (1975).
[45] G. M. Lankhuijzen and L. D. Noordam, Phys. Rev. Lett. **76**, 1784 (1996).
[46] C. Guet and W. R. Johnson, Phys. Rev. A **44**, 1531 (1991).
[47] H. Metcalf and P. van der Straten, Phys. Rep. **244**, 203 (1994).
[48] K. Sengstock and W. Ertmer 1995, Adv. At. Mol. Opt. Phys. **35**, 1 (1995).
[49] G. Alber, Phys. Rev. Lett. **69**, 3045 (1992); **70**, 2200 (1993).
[50] G. Alber and W. T. Strunz, Phys. Rev. A **50**, R3577 (1994).
[51] K. Gottfried, *Quantum Mechanics, Vol. I: Fundamentals* (W. A. Benjaminm, Reading, 1966).
[52] G. Alber, H. Ritsch, and P. Zoller, Phys. Rev. A **34**, 1058 (1986).
[53] W. S. Warren, H. Rabitz, and M. Dahleh, Science **259**, 1581 (1993).